AGU PUBLICATIONS

JGR

Journal of Geophysical Research: Solid Earth

RESEARCH ARTICLE
10.1002/2015JB012455

Key Points:
- Thermal anomaly beneath the Bentley Trench is consistent with Neogene extension
- Marie Byrd Land thermal anomaly supports anomalously high regional topography
- Ellsworth-Whitmore lithosphere is distinct relative to the study region

Correspondence to:
A. J. Lloyd,
a.j.lloyd@go.wustl.edu

Citation:
Lloyd, A. J., D. A. Wiens, A. A. Nyblade, S. Anandakrishnan, R. C. Aster, A. D. Huerta, T. J. Wilson, I. W. D. Dalziel, P. J. Shore, and D. Zhao (2015), A seismic transect across West Antarctica: Evidence for mantle thermal anomalies beneath the Bentley Subglacial Trench and the Marie Byrd Land Dome, *J. Geophys. Res. Solid Earth*, *120*, 8439–8460, doi:10.1002/2015JB012455.

Received 17 AUG 2015
Accepted 2 NOV 2015
Accepted article online 12 NOV 2015
Published online 15 DEC 2015

A seismic transect across West Antarctica: Evidence for mantle thermal anomalies beneath the Bentley Subglacial Trench and the Marie Byrd Land Dome

Andrew J. Lloyd[1], Douglas A. Wiens[1], Andrew A. Nyblade[2], Sridhar Anandakrishnan[2], Richard C. Aster[3], Audrey D. Huerta[4], Terry J. Wilson[5], Ian W. D. Dalziel[6], Patrick J. Shore[1], and Dapeng Zhao[7]

[1]Department of Earth and Planetary Sciences, Washington University in St. Louis, St. Louis, Missouri, USA, [2]Department of Geosciences, Pennsylvania State University, University Park, Pennsylvania, USA, [3]Department of Geosciences, Colorado State University, Fort Collins, Colorado, USA, [4]Department of Geological Sciences, Central Washington University, Ellensburg, Washington, USA, [5]Byrd Polar Research Center and School of Earth Sciences, Ohio State University, Columbus, Ohio, USA, [6]Institute for Geophysics, Jackson School of Geosciences, University of Texas at Austin, Austin, Texas, USA, [7]Department of Geophysics, Tohoku University, Sendai, Japan

Abstract West Antarctica consists of several tectonically diverse terranes, including the West Antarctic Rift System, a topographic low region of extended continental crust. In contrast, the adjacent Marie Byrd Land and Ellsworth-Whitmore mountains crustal blocks are on average over 1 km higher, with the former dominated by polygenetic shield and stratovolcanoes protruding through the West Antarctic ice sheet and the latter having a Precambrian basement. The upper mantle structure of these regions is important for inferring the geologic history and tectonic processes, as well as the influence of the solid earth on ice sheet dynamics. Yet this structure is poorly constrained due to a lack of seismological data. As part of the Polar Earth Observing Network, 13 temporary broadband seismic stations were deployed from January 2010 to January 2012 that extended from the Whitmore Mountains, across the West Antarctic Rift System, and into Marie Byrd Land with a mean station spacing of ~90 km. Relative *P* and *S* wave travel time residuals were obtained from these stations as well as five other nearby stations by cross correlation. The relative residuals, corrected for both ice and crustal structure using previously published receiver function models of crustal velocity, were inverted to image the relative *P* and *S* wave velocity structure of the West Antarctic upper mantle. Some of the fastest relative *P* and *S* wave velocities are observed beneath the Ellsworth-Whitmore mountains crustal block and extend to the southern flank of the Bentley Subglacial Trench. However, the velocities in this region are not fast enough to be compatible with a Precambrian lithospheric root, suggesting some combination of thermal, chemical, and structural modification of the lithosphere. The West Antarctic Rift System consists largely of relative fast uppermost mantle seismic velocities consistent with Late Cretaceous/early Cenozoic extension that at present likely has negligible rift related heat flow. In contrast, the Bentley Subglacial Trench, a narrow deep basin within the West Antarctic Rift System, has relative *P* and *S* wave velocities in the uppermost mantle that are ~1% and ~2% slower, respectively, and suggest a thermal anomaly of ~75 K. Models for the thermal evolution of a rift basin suggest that such a thermal anomaly is consistent with Neogene extension within the Bentley Subglacial Trench and may, at least in part, account for elevated heat flow reported at the nearby West Antarctic Ice Sheet Divide Ice Core and at Subglacial Lake Whillans. The slowest relative *P* and *S* wave velocity anomaly is observed extending to at least 200 km depth beneath the Executive Committee Range in Marie Byrd Land, which is consistent with warm possibly plume-related, upper mantle. The imaged low-velocity anomaly and inferred thermal perturbation (~150 K) are sufficient to support isostatically the anomalous long-wavelength topography of Marie Byrd Land, relative to the adjacent West Antarctic Rift System.

1. Introduction

West Antarctica is geologically unexplored except where nunataks and volcanic edifices protrude through the West Antarctic ice sheet. Knowledge of the West Antarctic Rift System (WARS), one of Earth's largest regions of extended continental crust [*Behrendt et al.*, 1991], the volcanic province of Marie Byrd Land [*LeMasurier*, 1990], and the major West Antarctic crustal blocks [*Dalziel and Elliot*, 1982] is thus highly dependent on geophysical studies, with seismological studies offering the greatest resolution of large-scale crust

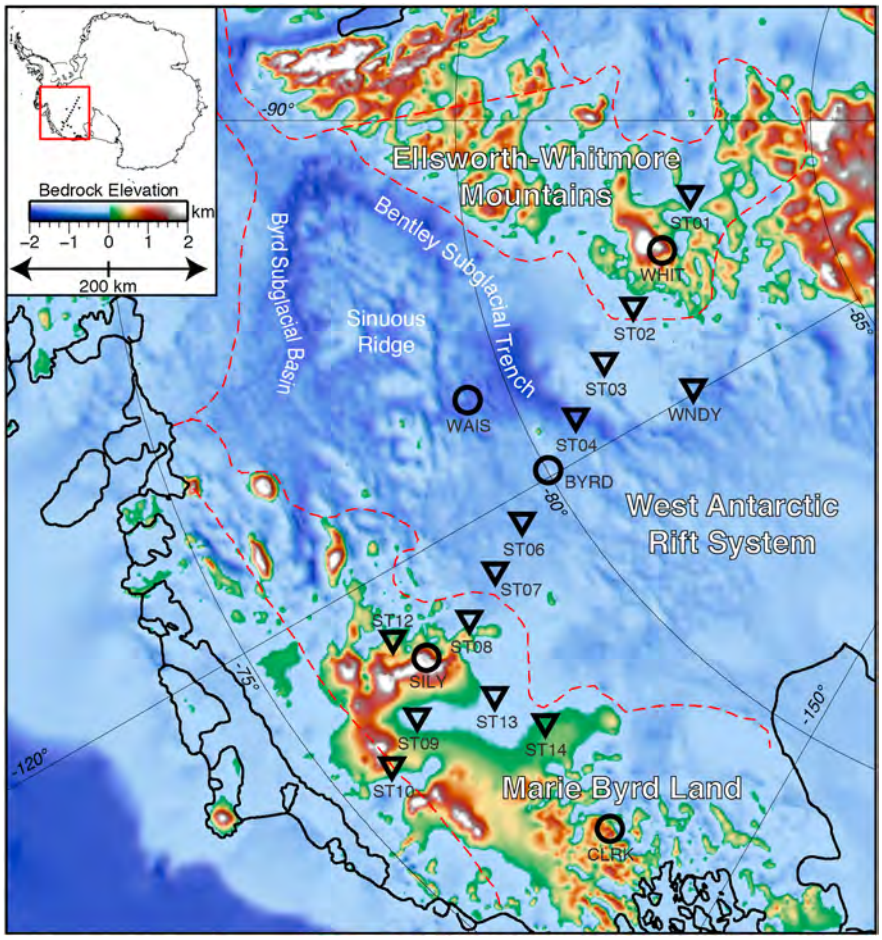

Figure 1. Map of the seismic component of the POLENET/A-NET experiment used in this study, in which circles indicate long-term backbone seismic stations and triangles indicate temporary transect seismic stations. The dashed red lines delineate the major crustal blocks of West Antarctica [*Dalziel and Elliot*, 1982]. The modern bedrock topography is from BEDMAP2 [*Fretwell et al.*, 2013].

and mantle structure. Antarctic field and instrumentation challenges have, until recently, limited broadband seismographic coverage to science bases, smaller-scale temporary experiments, and a single sparse larger-scale network in central West Antarctica (The Antarctic Network of Unattended Broadband Seismometers - ANUBIS 1999–2001) [e.g., *Winberry and Anandakrishnan*, 2003].

Regional seismological studies can offer unique constraints on the structure and tectonic processes of West Antarctica. These include, but are not limited to, lithospheric structure and boundaries of the major West Antarctic crustal blocks previously delineated on the basis of the exposed outcrop geology, near-surface geophysics, and sub-ice topography [e.g., *Dalziel and Elliot*, 1982]. Separating these crustal blocks is thinned continental crust of the eastern WARS that has been little studied in comparison to its Ross Sea counterpart where marine studies can be preformed. Within the eastern WARS narrow deep basins that are topographically similar to the mid-Miocene Terror Rift in the Ross Sea [e.g., *Fielding et al.*, 2008] are observed in the bedrock topography (Figure 1). These eastern WARS basins have been proposed to also be zones of focused Neogene extension [*Winberry and Anandakrishnan*, 2004; *LeMasurier*, 2008; *Jordan et al.*, 2010], but little temporal constraints or information on crustal and mantle structure has, until recently, existed for these structures. Past Cenozoic and active magmatism has been geophysically inferred beneath the West Antarctic ice sheet [e.g., *Blankenship et al.*, 1993; *Behrendt*, 1999; *Lough et al.*, 2013] and is exposed within the Marie Byrd Land (MBL) province [*LeMasurier and Rex*, 1989]. Knowledge of the lateral variations in mantle seismic velocities at regional scales can potentially constrain mantle thermal variations related to volcanism, rifting, and other tectonic processes, in addition to delineating the major lithospheric domains of West Antarctica.

Imaging mantle structure beneath West Antarctica at regional scales is important to understand better not only the structure and tectonic processes, but also the interactions of the solid earth with the cryosphere. For example, the mantle seismic structure can provide constraints on basal heat flow [*Shapiro and Ritzwoller*, 2004], which fundamentally affects whether basal ice is at the pressure-melting point [*Pollard et al*., 2005]. Elevated upper mantle temperature will give rise to higher basal heat flow, resulting in sub-ice water that reduces basal friction [e.g., *Alley*, 1989] and has a first-order effect on coupled ice sheet climate models [e.g., *Deconto and Pollard*, 2003]. Seismic velocities also provide important constraints on mantle viscosity, which controls the magnitude and timescales of the isostatic response to glacial loading and unloading [e.g., *Walcott*, 1970; *Ivins and James*, 2005]. Although past models of glacial isostatic adjustment used uniform upper mantle viscosity models, the strong lateral variations in Antarctic mantle structure in previous continental-scale studies [e.g., *Ritzwoller et al*., 2001] suggests that lateral variations in mantle viscosity are highly important for understanding glacial isostatic adjustment, as well as current and past ice mass loss [*Ivins and James*, 2005; *A et al*., 2013; *van der Wal et al*., 2015].

The deployment of broadband seismic stations as part of the Polar Earth Observing Network (POLENET/A-NET) across West Antarctica starting in late 2007 provides an opportunity to image seismically the crust and mantle underpinnings of the principal geologic features. These features can now be imaged at a wholly new level of resolution due in part to the installation of a denser transect that operated between January 2010 to January 2012 (Figure 1). Here we present the first relative regional *P* and *S* body wave tomography models of the central West Antarctic upper mantle and discuss the constraints these models place upon the structure and tectonic processes, as well as heat flow at the base of the ice sheet and mantle viscosity [e.g., *Pollard et al*., 2005; *Steffen et al*., 2006].

2. Background

2.1. Tectonic Development of West Antarctica

West Antarctica consists of at least four distinct crustal blocks that have undergone staggered reorganization since the mid-Jurassic [*Dalziel and Elliot*, 1982; *Veevers*, 2012], leading to widespread extension of continental lithosphere in multiple stages to form the Weddell Sea [e.g., *Dalziel et al*., 2013] and the WARS [*Siddoway*, 2008; *Wilson and Luyendyk*, 2009]. MBL, Thurston Island-Eights Coast, and the Antarctic Peninsula along with Zealandia were fore arc and magmatic arc terranes inboard of the subducting Phoenix plate at the convergent central Pacific margin of Gondwanaland [*Grunow et al*., 1991; *Mukasa and Dalziel*, 2000]. The fourth West Antarctic crustal block, the Ellsworth-Whitmore mountains crustal block, was originally located between southernmost Africa and East Antarctica within Gondwanaland [*Schopf*, 1969; *Grunow et al*., 1987; *Randall and Mac Niocaill*, 2004].

The breakup of Gondwanaland, beginning in the mid-Jurassic with the opening of the Somali Basin, Mozambique Basin, and Weddell Sea, was accommodated by the counterclockwise rotation and translation of the Ellsworth-Whitmore mountains crustal block [*Grunow et al*., 1987; *Randall and Mac Niocaill*, 2004; *Dalziel et al*., 2013]. This process may have been set in motion by a mantle plume interacting and ultimately thermochemically breaking the subducted Phoenix slab, leading to slab retreat along the central Pacific margin of Gondwanaland and extreme extension along low-angle detachment faults within the back arc [*Dalziel et al*., 2013]. Most of the exposed outcrops in the Ellsworth-Whitmore mountains crustal block consist of Cambrian-Permian sedimentary rocks underlain by a Precambrian basement [e.g., *Dalziel and Elliot*, 1982]. However, some nunataks, like the Pirrit Hills, Nash Hills, and Whitmore Mountains, are largely composed of mid-Jurassic granites that were emplaced following rotation [*Grunow et al*., 1987]. These within-plate granites may be petrogenetically related to the nearly contemporaneous Ferrar large igneous province [*Storey et al*., 1988] that spans the length of the present-day Transantarctic Mountains and whose emplacement may be linked to the origin of the WARS [*Elliot and Fleming*, 2004].

However, it was not until the Late Cretaceous, during the final phase of oblique subduction, that significant intracontinental extension occurred within the WARS itself [*Luyendyk*, 1995]. During this stage (~105 Ma to ~85 Ma) the stress regime transitioned from transpressional to transtensional in response to the opening of a slab window [*Luyendyk*, 1995] and resulted in broadly distributed extension as MBL, Thurston Island-Eights Coast, and Zealandia drifted away from East Antarctica along the WARS [*Luyendyk et al*., 1996]. By 83 Ma Zealandia broke away from West Antarctica in what was a distinct extensional event

[*Siddoway*, 2008]. Tectonic activity within the WARS continued into the Cenozoic but is not fully understood due to the West Antarctic ice sheet obscuring the bedrock geology.

Within the Ross Sea sector of the WARS approximately 150 km of extension occurred between 68 and 46 Ma, as constrained by the seafloor spreading record and plate circuit calculations [*Cande and Stock*, 2004; *Wilson and Luyendyk*, 2009]. In contrast, Eocene and Oligocene deformation within the eastern WARS is characterized as oblique convergence [*Granot et al*., 2013] or dextral strike-slip motion [*Müller et al*., 2007]. This is constrained by aeromagnetic data from the Adare and Northern Basins in the Ross Sea [*Granot et al*., 2013] and East Antarctic-Australia-Pacific-West Antarctic plate circuit closure models that have been combined with estimates of West Antarctic crustal thinning [*Müller et al*., 2007], respectively. A pulse of mid-Miocene, ~17 Ma, rifting activity characterized by near-vertical normal faulting marks the last phase of extension within the Adare Basin [*Granot et al*., 2010]. Subsequent extension is observed within the Terror Rift [*Henrys et al*., 2008; *Fielding et al*., 2008], near Ross Island, but is absent within the Adare basin, suggesting a pronounced kinematic change of the rift system [*Granot et al*., 2010]. This event may also be linked with inferred Neogene reactivation of subglacial basins (e.g., Bentley Subglacial Trench and Byrd Subglacial Basin) within the eastern WARS [*Winberry and Anandakrishnan*, 2004; *LeMasurier*, 2008; *Jordan et al*., 2010; *Bingham et al*., 2012; *Chaput et al*., 2014]. At present the WARS appears to be dormant, as local seismic networks observe only very sparse tectonic seismicity within or adjacent to the rift system [*Winberry and Anandakrishnan*, 2003; *Lough*, 2014] and GPS stations installed on nunataks throughout West Antarctica and the Transantarctic Mountains indicate no resolvable extensional motion [*Donnellan and Luyendyk*, 2004; *Wilson et al*., 2015].

There has been much speculation over the tectonic origin of the deep subglacial valleys in West Antarctica, including the very prominent Bentley Subglacial Trench and the Byrd Subglacial Basin. Bedrock topography, magnetic and gravity anomalies, and thin crust have all been used to suggest these features may be Cenozoic rift basins [*Winberry and Anandakrishnan*, 2004; *LeMasurier*, 2008; *Jordan et al*., 2010; *Bingham et al*., 2012; *Chaput et al*., 2014]. Alternatively, others have suggested that these tectonic features (e.g., Bentley Subglacial Trench and Byrd Subglacial Basin) may represent Oligocene transcurrent faults that have been reactivated under extension during post mid-Miocene rifting [*Granot et al*., 2013] or that they formed during the main phase of WARS extension during the Cretaceous [*Trey et al*., 1999]. Geologically recent extension along these rift basins may aid in accounting for high geothermal heat flow recently inferred in parts of West Antarctica [*Clow et al*., 2012; *Schroeder et al*., 2014; *Fisher et al*., 2015].

Cenozoic volcanism is observed within MBL and along the Transantarctic Mountains [e.g., *LeMasurier*, 1990], as well as inferred using geophysical methods to be widespread beneath the West Antarctic ice sheet and in the Ross Sea [e.g., *Blankenship et al*., 1993; *Behrendt*, 1999]. In particular, the MBL volcanic dome, a region of high topography north of the main axis of the WARS, penetrates and lies unconformably over Paleozoic rocks that are intruded by late Paleozoic and Mesozoic granites. This unconformity, observed at several nunataks, is inferred to represent a single erosional surface that has undergone a maximum of ~3 km of uplift since the onset of MBL volcanism during the Oligocene [*LeMasurier and Landis*, 1996]. Seismic crustal studies of MBL indicate thickened crust relative to the eastern WARS, but also that crustal isostatic support is nonetheless insufficient to account for the topographic difference between the two regions [*Winberry and Anandakrishnan*, 2004; *Chaput et al*., 2014], and that additional support from a low-density mantle source is required.

The MBL volcanic complex consists of extensive alkaline basaltic rocks topped by 18 major subaerial polygenetic shield and stratovolcanoes [*LeMasurier and Rex*, 1989]. Many of these volcanoes are within one of three linear volcanic chains, such as the Executive Committee Range, that trend in different directions and do not agree with plate motion. It has been proposed that these patterns reflect anisotropic stress conditions that tectonically drive magma by fracture propagation within the lithosphere, and which may exploit preexisting N-S and E-W fractures in the region [*LeMasurier and Rex*, 1989; *Panter et al*., 1994; *Paulsen and Wilson*, 2010]. The cause of volcanism is highly debated and has been attributed to an upper mantle hotspot or a mantle plume [*LeMasurier and Landis*, 1996; *Behrendt*, 1999], in which the latter is loosely define as a thermal upwelling extending into the lower mantle [e.g., *Campbell and Griffiths*, 1990; *Sleep*, 1990; *Schmandt et al*., 2012; *French and Romanowicz*, 2015]. Alternatively, more exotic mechanisms such as Rayleigh-Taylor instabilities created by slab detachment in the Late Cretaceous have been suggested, possibly interacting with metasomatized lithosphere to explain widespread Cenozoic volcanism in West Antarctica and within portions of the southwest Pacific [*Finn et al*., 2005].

2.2. Upper Mantle and Crustal Structure of West Antarctica

The first 3-D seismological models of the Antarctic plate used fundamental mode Rayleigh waves [*Roult et al*., 1994; *Danesi and Morelli*, 2001] or both fundamental mode Rayleigh and Love waves [*Ritzwoller et al*., 2001] from a handful of global seismographic stations to produce low-resolution images to approximately 400 km depth. These studies produced shear wave velocity maps that clearly revealed strong mantle asymmetry of the continent, with fast upper mantle velocities beneath the East Antarctic shield and slow velocities beneath West Antarctica. *Sieminski et al*. [2003] found similar seismic velocities down to 200 km depth, and through the use of higher-order mode Rayleigh waves constrained shear wave velocities down to 600 km depth. In this model slow shear wave velocities in the asthenosphere extend into the transition zone beneath the Amundsen Sea-Marie Byrd Land coast, the Ross Sea, and the Balleny Islands. *An et al*. [2015] improved the resolution of continental-scale fundamental mode Rayleigh wave tomographic models using additional recent seismic stations. However, the lateral resolution of these models is insufficient to reveal features associated with the tectonic structure of Antarctica at the scale of the West Antarctic crustal blocks.

The TAMSEIS experiment provided the first regional-scale glimpse of the upper mantle seismic structure, focusing on the vicinity of Ross Island, revealing a region of thin lithosphere and thick, highly anelastic asthenosphere [*Lawrence et al*., 2006a, 2006b; *Watson et al*., 2006]. More recently, the POLENET/A-NET broadband seismic deployments have allowed much of the upper mantle beneath West Antarctica to be imaged by fundamental mode Rayleigh waves at regional scales down to depths near 300 km (D. S. Heeszel et al., Shear velocity structure of Central and West Antarctica from Array Analysis of Rayleigh Wave Phase Velocities, submitted to *Journal of Geophysical Research: Solid Earth*, 2015, hereafter referred to as D. S. Heeszel et al., submitted manuscript, 2015) and by absolute *P* wave travel time tomography [*Hansen et al*., 2014]. In both models, globally slow seismic velocities are observed beneath the eastern WARS and MBL [*Hansen et al*., 2014; D. S. Heeszel et al., submitted manuscript, 2015]. In particular, the slowest vertically polarized shear wave velocities are observed beneath MBL centered on the Executive Committee Range; however, the depth extent of the anomaly cannot be resolved from fundamental mode Rayleigh waves (D. S. Heeszel et al., submitted manuscript, 2015). The absolute *P* wave tomography has limited resolution but shows a region of slow velocities beneath MBL and part of the eastern WARS extending to ~800 km depth [*Hansen et al*., 2014]. However, little variation in transition zone thickness is reported beneath the region, suggesting that under normal mantle assumptions, there is no regional mantle thermal anomaly at depths greater than 400 km associated with this feature [*Emry et al*., 2015].

Seismic and gravity studies have provided constraints on crustal structure, especially crustal thickness, across West Antarctica at various scales. Surface wave studies and GRACE gravity inversions suggest that West Antarctica has a widespread average crustal thickness of 25 km to 27 km [*Evison et al*., 1960; *Ritzwoller et al*., 2001] and ~30 km [*Block et al*., 2009], respectively. Passive seismological studies utilizing receiver function and/or ambient noise techniques offer much better resolution of Moho depth [*Winberry and Anandakrishnan*, 2004; *Sun et al*., 2013; *Chaput et al*., 2014] showing crustal thicknesses of 19–28 km within the eastern WARS, ~30 km within the Ellsworth-Whitmore mountains crustal block in the vicinity of the Whitmore Mountains, and 25–32 km within MBL. These estimates are consistent with crustal thicknesses estimated across the whole of West Antarctica by inverting satellite gravity data that was constrained with crustal thicknesses from receiver functions and active source seismic surveys [*O'Donnell and Nyblade*, 2014]. *P*-to-*S* receiver functions indicate that the thinnest crust, ~19 km, [*Winberry and Anandakrishnan*, 2004; *Chaput et al*., 2014] can be found beneath the narrow deep basins of the eastern WARS (Figure 1). Modeling of airborne gravity data suggests that this trend is pervasive throughout the Bentley Subglacial Trench, Byrd Subglacial Basin, and the Pine Island Glacier Rift [*Jordan et al*., 2010], consistent with extensional/pure shear focused crustal-scale thinning associated with these features.

3. Data and Methodology

3.1. Seismic Data

This study utilizes a subset of broadband seismic data collected by the Antarctic component of the Polar Earth Observing Network (POLENET/A-NET) in central West Antarctica between January 2010 and January 2012 (Figure 1). The POLENET/A-NET experiment consists of a sparse backbone network and a dense transect. Installation of the seismic backbone network began during the 2007/2008 Antarctic field season and was

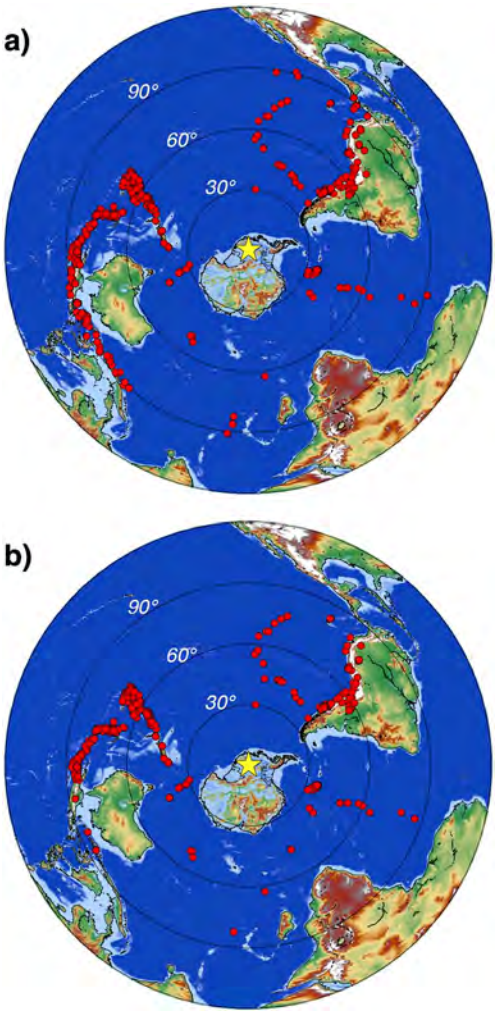

Figure 2. Event distribution used in the (a) *P* and (b) *S* wave tomography models. The yellow star indicates the center of the array, the red dots indicate earthquake locations, and the concentric circles mark distances in 30° increments. Global surface topography and Antarctic bedrock topography [*Fretwell et al.*, 2013] are shown in the same color scale as Figure 1.

completed during the 2010/2011 Antarctic field season. Many of the 24 backbone seismic stations are colocated with continuously recording GPS stations installed on nunataks throughout West Antarctica and in the Transantarctic Mountains [*Wilson et al.*, 2015]. Each station is equipped with a Quanterra Q330 data logger and either a cold-rated Guralp CMG-3T (120 s) or Nanometrics T240 (240 s) broadband seismometer. The stations record continuous 40 sample/s seismic data with power provided by lead-acid batteries that are recharged during the austral summer by two or three 100 W solar panels. Bandwidth and power limitations prohibit the transmission of real time data; however, each backbone station sends a daily "state of health" report via a Xeos Iridium Constellation satellite modem.

The denser seismic transect consisted of 13 temporary seismic stations that operated from January 2010 to January 2012. Twelve temporary stations in combination with three backbone stations formed two linear arrays with a mean interstation separation of ~90 km. The first array consisted of 10 transect stations and three backbone stations that stretched ~1100 km from the Whitmore Mountains to near the MBL coast. The remaining three transect stations formed a ~270 km long linear array that crossed the first near Mount Sidley, in MBL (Figure 1). In addition, two backbone stations and one temporary station near the two linear arrays are utilized. Each of the transect stations consisted of the same sensor and data logger as the backbone stations, but were powered by supplemental lithium batteries during the austral winter and three 20 W solar panels during the austral summer.

3.2. Determination of Relative Travel Time Residuals

Relative travel time residuals were determined using the adaptive stacking algorithm of *Rawlinson and Kennett* [2004] for teleseismic *P* and *S* phases from earthquakes with $M_w \geq 5.5$ at distances of 30°–90° and 30°–85°, respectively (Figure 2). Both event distributions provide wide azimuthal coverage. However, the majority of earthquakes in this range occur along the South American subduction zone or along the Pacific-Indian plate boundary from Tonga/Fiji to Sumatra. The *P* wave and *S* wave velocity models in this study are constrained by relative travel time residuals along 5010 *P* wave raypaths from 494 events and by 3728 *S* wave raypaths from 389 events.

P and *S* relative travel time residuals are computed from the vertical and transverse time series components, respectively. Initially, the instrument response is removed and a body wave band Butterworth band-pass filter is applied (*P*: 0.4–2.0 Hz; *S*: 0.04–0.2 Hz). For each event the waveforms are windowed and aligned about

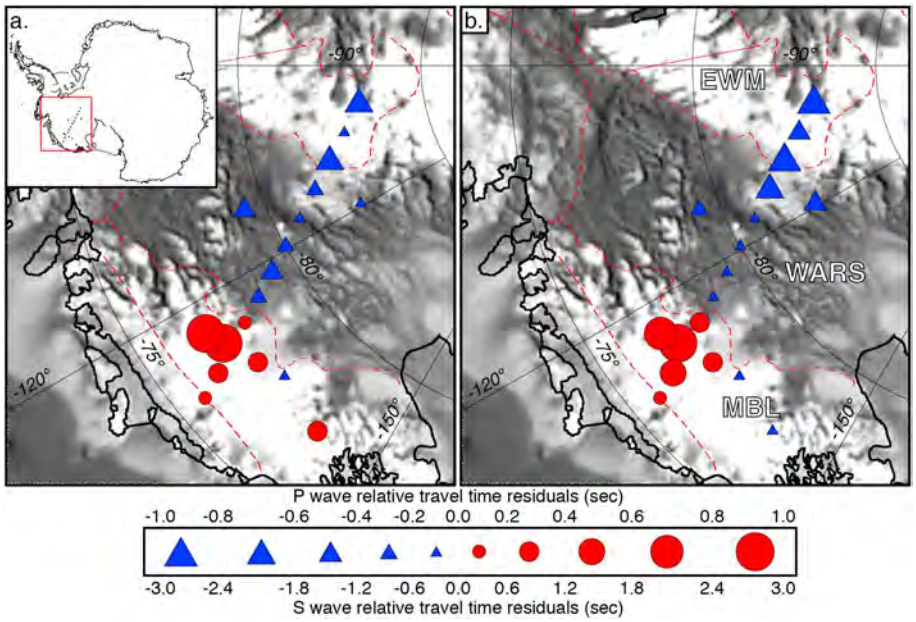

Figure 3. Mode of the relative travel time residuals used in the (a) *P* and (b) *S* wave tomography model. Negative residuals (blue triangles) indicate advanced arrivals relative to the array average, while positive residuals (red circles) indicate delayed arrivals relative to the array average. Darker shades indicate lower bedrock topography [*Fretwell et al*., 2013]. Abbreviations are as follows: MBL, Marie Byrd Land; WARS, West Antarctic Rift System; EWM, Ellsworth-Whitmore mountains crustal block.

the theoretical arrival time calculated from the IASP91 velocity model [*Kennett and Engdahl*, 1991] within the mantle and a preferred ice and crustal velocity model that best fits receiver functions at each station as determined by *Chaput et al*. [2014]. The receiver function analysis incorporated iterative forward modeling combined with Bayesian Markov chain Monte Carlo methodology to resolve ice and crustal structure [*Chaput et al*., 2014].

The windowed waveforms are perturbed in the time domain in order to minimize a cubic difference misfit function,

$$\Psi_{i\in[1,10]} = \sum_{j=1}^{M} \left| \left[\frac{1}{N} \sum_{n=1}^{N} u_n\left(t_j - \tau_{n,i-1}\right) \right] - u_n\left(t_j - \tau_{n,i}\right) \right|^3, \tag{1}$$

where i is the iteration number, M is the number of samples in the waveform, N is the number of waveforms, u_n is the n-th waveform, and $\tau_{n,i}$ is the time shift required to minimize the misfit function at the i-th iteration. In general, the solution converges after a few iterations, and 10 iterations were sufficient in all cases. The relative travel time residuals are then defined as

$$T_n = \tau_{n,10} - \frac{1}{N} \sum_{n=1}^{N} \tau_{n,10}. \tag{2}$$

Note that the relative travel time residuals are further constrained by removing the mean and are thus relative to the regional mean as sampled by the seismic network.

Rawlinson and Kennett [2004] observed that the shape of the misfit function correlates with the similarity and bandwidth of the waveform, such that high signal-to-noise waveforms produce a narrower and deeper minimum. Given this behavior, an a priori error estimate can be defined as the smallest time shift required that is sufficient to increase the misfit function minimum by a factor of ε, which is taken to be 1.15 in this study. The a priori error estimates are used in two main ways. First, to identify a preferred window length (*P*: 15 s, 21 s, or 27 s; *S*: 30 s, 36 s, or 42 s) for each event, which is taken to be the shortest window that minimizes the L_1 norm of the a priori error estimates. Second, to eliminate waveforms having low signal-to-noise rations, as identified by an a priori error estimate greater than 0.5 s.

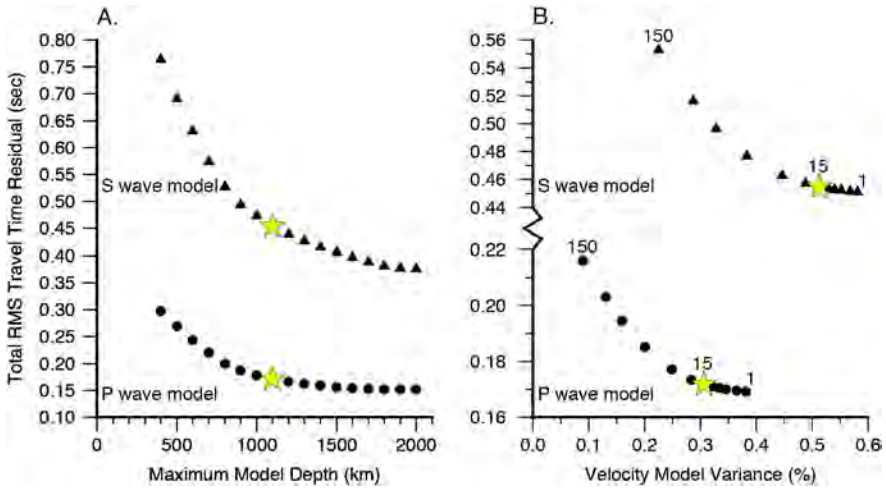

Figure 4. (a) Trade-off curve between the total root-mean-square (RMS) travel time residual and the maximum model depth for both the *P* and *S* wave tomography model (circles and triangles, respectively). Both damping (*P*/*S*: 15/15) and smoothing (*P*/*S*: 0.001/0.001) are fixed. (b) Trade-off curve between the total RMS travel time residual and the model variance used in choosing the preferred damping coefficient. Both the maximum model depth (1100 km) and the smoothing coefficient are fixed. In all four curves the yellow star indicates the preferred solution.

The range of the time shift parameter τ is important to this process. For example, if τ is restricted too narrowly, the minimum in the misfit function (equation (1)) may not be reached, resulting in relative travel time residuals piling up at the limits of the search range. Alternatively, if τ is insufficiently restricted, the potential for cycle skipping across the seismic waveforms is increased, particularly for those with a lower signal-to-noise ratio and/or limited bandwidth. In this study, based on empirical exploration of the data, τ was restricted to ±4.0 s and ±8.0 s for *P* and *S* phases, respectively, resulting in well-defined peaks in the relative travel time residual distribution for each station. The mode of both the *P* and *S* relative travel time residual distributions ranges approximately from ±1.0 s to ±3.0 s, respectively, and shows a similar geographic pattern (Figure 3). Lastly, outlier residuals removed from the station mode by more than the range of the relative travel time residual modes (*P*: 2.0 s; *S*: 6.0 s) were excluded.

3.3. Inversion

P and *S* relative travel time residuals were utilized to produce independent *P* and *S* relative velocity models using a modified version of the code developed by *Zhao et al*. [1994]. Initially, all stations and earthquakes are rotated into a coordinate system in which the strike of the transect lies along the equator. The model space was laterally discretized with nodes every 0.5° and vertically discretized within the mantle with nodes every 25 km from 25 km depth (approximately the average Moho depth across the array) down to a depth of 800 km and with nodes every 50 km below that from 800 km to 1100 km depth. Trade-off curves were examined in order to determine the optimum model depth (Figure 4a) and optimum damping parameter (Figure 4b). A regularizing second derivative smoothing operator was applied to produce a smooth model.

The method of *Zhao et al*. [1994] assumes an infinite frequency wave but does not directly solve the ray equations. Instead, the raypaths are iteratively determined using the pseudobending algorithm of *Um and Thurber* [1987] in regions of continuous velocity and using Snell's law at any velocity discontinuities, as discussed by *Zhao et al*. [1992]. For each raypath the partial derivatives of the travel times with respect to velocity model parameters are determined, and a system of linear equations relating the relative travel time residuals to the medium parameters are constructed following *Aki and Lee* [1976], *Thurber* [1983], and *Zhao* [1991]. Using a LSQR conjugate gradient algorithm [*Paige and Saunders*, 1982] that includes damping and the regularization constraints imposed by a second derivative smoothing matrix, this large sparse system is solved for the relative node velocities. Synthetic tests are used to interrogate the resolution of both models and are discussed in section 4.1. The preferred *P* and *S* wave velocity models reduce the variance of the relative travel time residuals, relative to the IASP91 background reference velocity model [*Kennett and Engdahl*, 1991], by ~91% and ~92%, respectively.

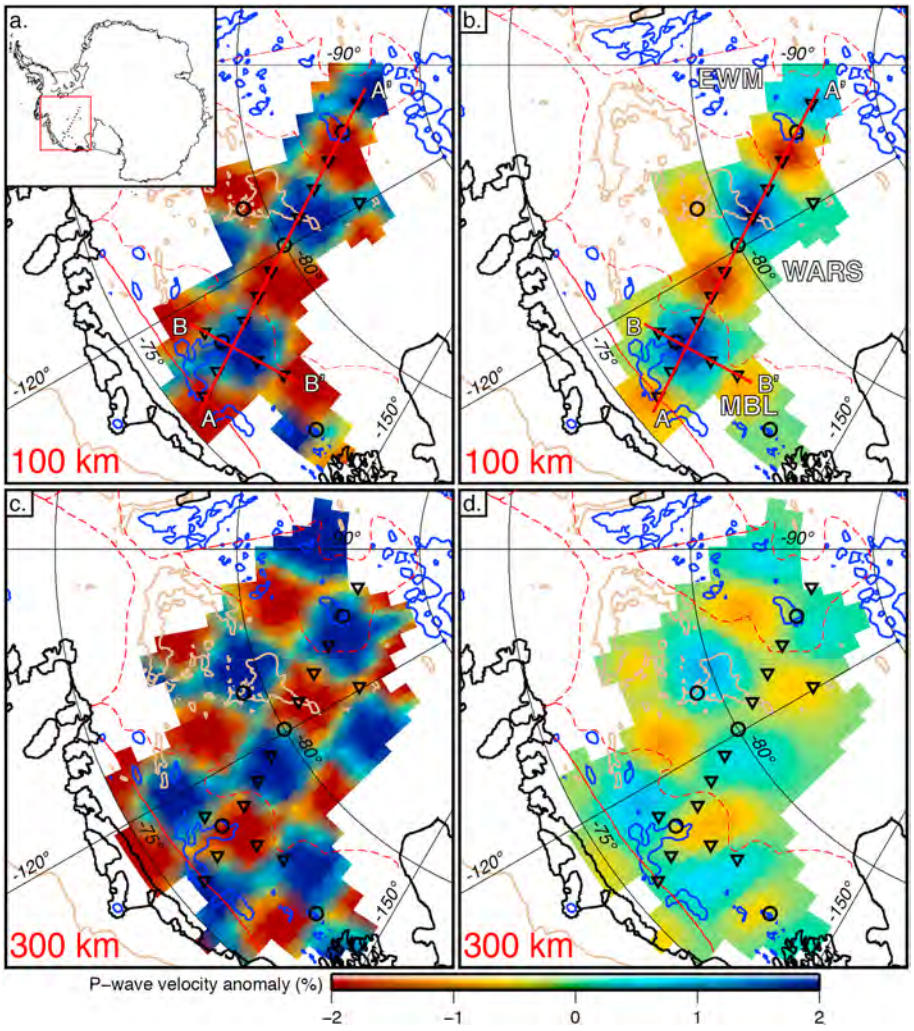

Figure 5. Horizontal slices through a *P* wave resolution test consisting of two layers of alternating checkers. The (a and c) input and (b and d) output models are shown for 100 and 300 km depth. Abbreviations are as follows: MBL, Marie Byrd Land; WARS, West Antarctic Rift System; EWM, Ellsworth-Whitmore mountains crustal block.

4. Results

4.1. *P* and *S* Wave Resolution Tests

Multiple tests were preformed to assess the resolution of both the *P* and *S* wave velocity models. Here we discuss the results from a subset of these tests consisting of input models with two layers of alternating checkered anomalies (δV_p: ±0.1%, ±0.2%, ±0.5%, or ±2.0%; δV_s: ±0.2%, ±0.5%, ±1.0%, or ±4.0%) having lateral dimensions of 1°, 1.5°, or 2° and a thickness of 200 km. In all instances the top of the upper layer was fixed at 25 km depth. Synthetic relative travel time residuals were calculated for each input model, and zero mean Gaussian random noise (*P*: $\sigma = 0.17$ s; *S*: $\sigma = 0.45$ s; consistent with the data) was added to the synthetic travel times prior to the inversion. A sample of one such test for both the *P* and *S* wave velocity model is shown in Figures 5–8.

P and *S* wave resolution tests consisting of two layers of checkered anomalies indicate that amplitude differences greater than 0.2% and 0.4%, respectively, over lateral length scales ≥~200 km are well resolved down to at least 400 km depth. At shorter length scales, ~100 km, the test pattern is only recovered at depths shallower than 200 km. However, the checkered pattern in the bottom layer exhibits significant resolution artifacts both laterally and vertically (Figures 5d, 6, 7d, and 8), as is expected due to the near vertical teleseismic raypaths. Thus, vertical resolution is poorer than horizontal resolution. In the best vertically resolved

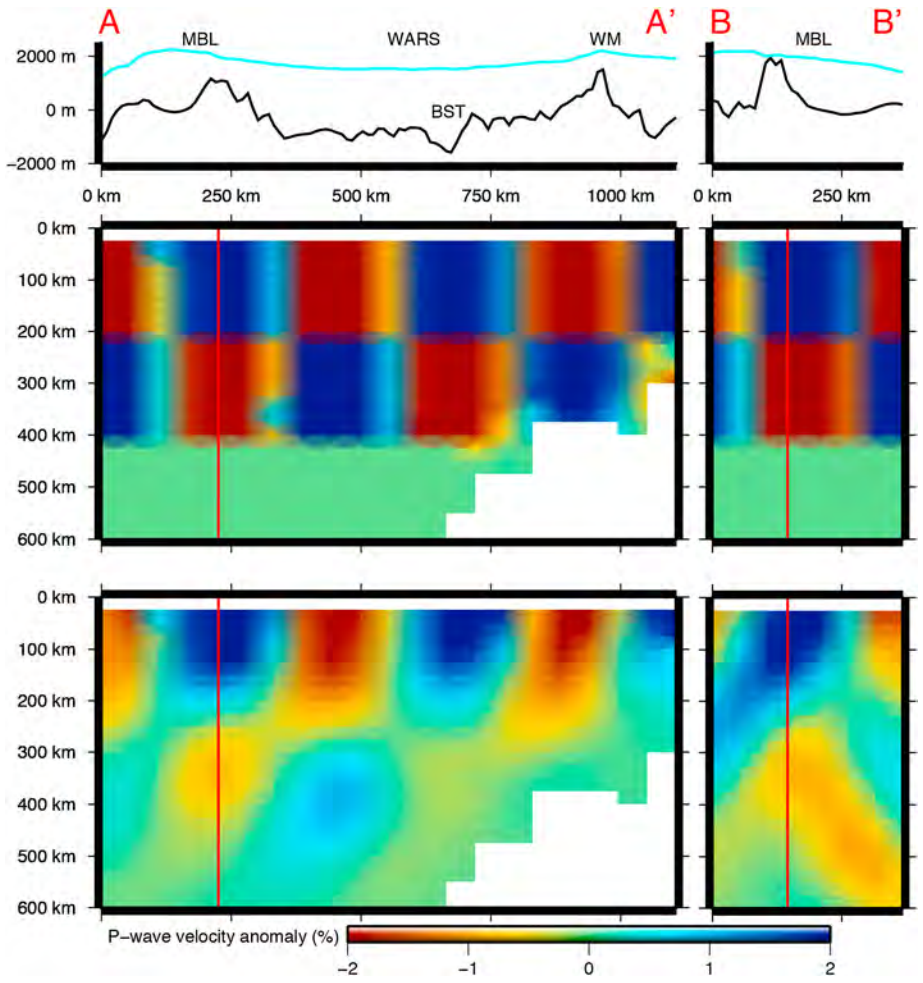

Figure 6. Vertical slices through a *P* wave resolution test consisting of two layers of alternating checkers. The (top) input and (bottom) output are shown for profiles A-A′ and B-B′, whose location is shown in Figures 5a and 5b. The vertical red line indicates the intersection of A-A′ and B-B′. Abbreviations are as follows: MBL, Marie Byrd Land; WARS, West Antarctic Rift System; BST, Bentley Subglacial Trench; WM, Whitmore Mountains.

regions, such as beneath eastern MBL, a minimum of 50 km of vertical smearing is observed (Figures 6 and 8). Farther to the south, vertical resolution becomes poorer due to increased gaps in raypath coverage. Anomaly amplitude recovery, for both the *P* and *S* wave resolution tests in the (best recovered) upper layer of checkers is ~60–80% (Figures 5–8). Peak amplitude recovery in the bottom layer is much more variable, ranging from 20% to 50%. At depths exceeding 400 km, additional resolution test variants indicate that both models become irresolvable.

Finally, several inversions of uncorrelated zero mean Gaussian random noise (*P*: $\sigma = 0.17$ s; *S*: $\sigma = 0.45$ s) were further conducted to assess velocity variations due to random propagation of data noise into the model. Corresponding peak differences in velocity (δV_p and δV_s) were ~0.3% and ~0.6%, respectively. Although general variations in δV_p and δV_s across the array were much smaller, a conservative approach suggests that the maximum variations in velocity that can be attributed to data noise are in this range.

4.2. *P* and *S* Wave Relative Velocity Models

Slices through the *P* and *S* wave relative velocity models (Figures 9–12) reveal velocity variations between ±2.0% and ±4.0%, respectively. The distribution of fast and slow velocities, relative to the model mean, is highly similar between the *P* and *S* models. The greatest resolved seismic heterogeneity in both cases is confined to the upper 250 km of the mantle and correlates loosely with the major West Antarctic crustal

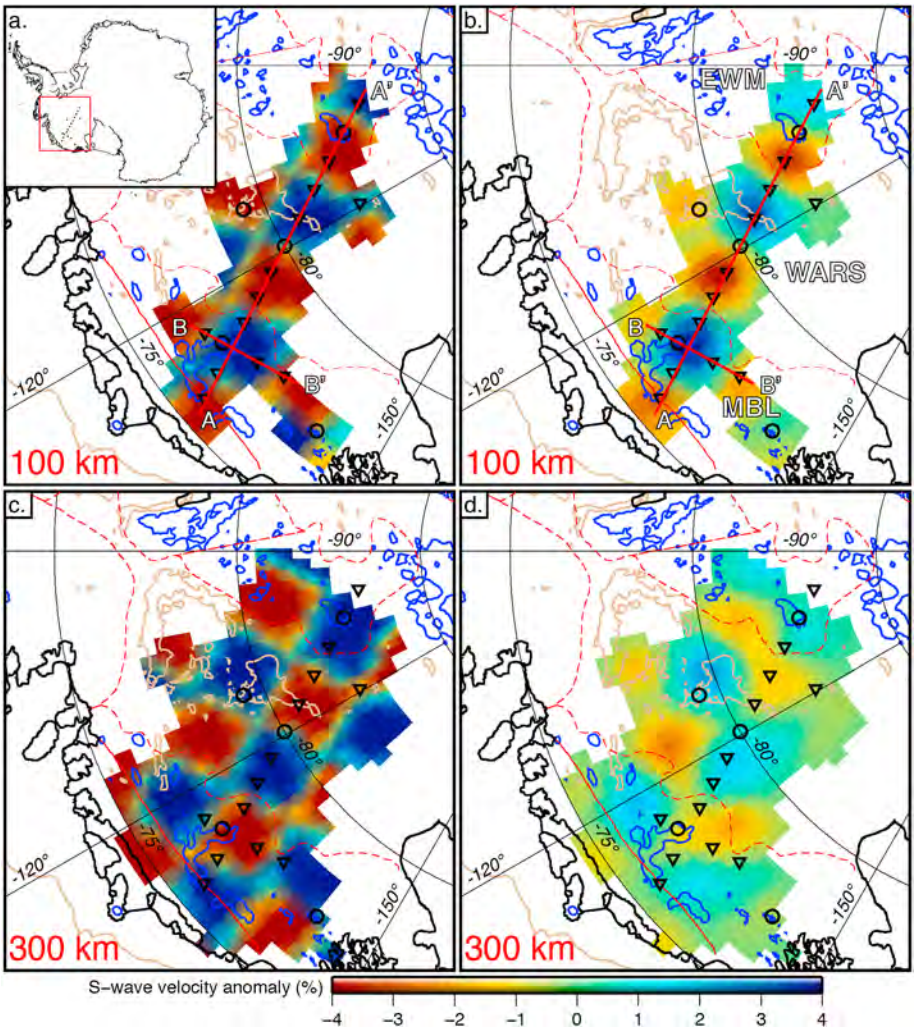

Figure 7. Horizontal slices through an *S* wave resolution test consisting of two layers of alternating checkers. The (a and c) input and (b and d) output models are shown for 100 and 300 km depth. Abbreviations are as follows: MBL, Marie Byrd Land; WARS, West Antarctic Rift System; EWM, Ellsworth-Whitmore mountains crustal block.

blocks [*Dalziel and Elliot*, 1982] and prominent physiographic features observed in the bedrock topography [*Fretwell et al*., 2013].

Beneath eastern MBL both models exhibit a very prominent region of slow velocities ($\delta V_p < -1.0\%$ and $\delta V_s < -2.0\%$) that extends to ~200 km depth and is centered beneath Mount Sidley in the Executive Committee Range (Figures 9–12). Resolution tests indicate at least 50 km of vertical smearing can be anticipated in this region of the model, suggesting that this anomaly is consistent with low velocities extending to only ~150 km depth but which could be substantially deeper. The lateral extent of the eastern MBL anomaly is poorly constrained to the geographic east due to the lack of seismic stations there, but in other directions, it is clearly confined to the vicinity of the Executive Committee Range.

Within the upper 200 km of the seismic transect across the eastern WARS and south of MBL, *P* and *S* wave velocity variations range from ~2.0% to ~0% and ~4.0% to ~−1.0%, respectively (Figures 9–12). The region can be further subdivided on the basis of the *P* and *S* wave velocity models into three domains from north to south. The first, extending from MBL to the northern flank of the Bentley Subglacial Trench is underlain by fast seismic velocities ($\delta V_p > 1.0\%$ and $\delta V_s \approx 1.0\%$) that extend to ~200 km depth. Second, as the bedrock topography deepens into the Bentley Subglacial Trench, fast *P* wave upper mantle seismic velocities decline to velocities near the model mean and to moderately low (~ −1.0%) shear wave velocities. These lower

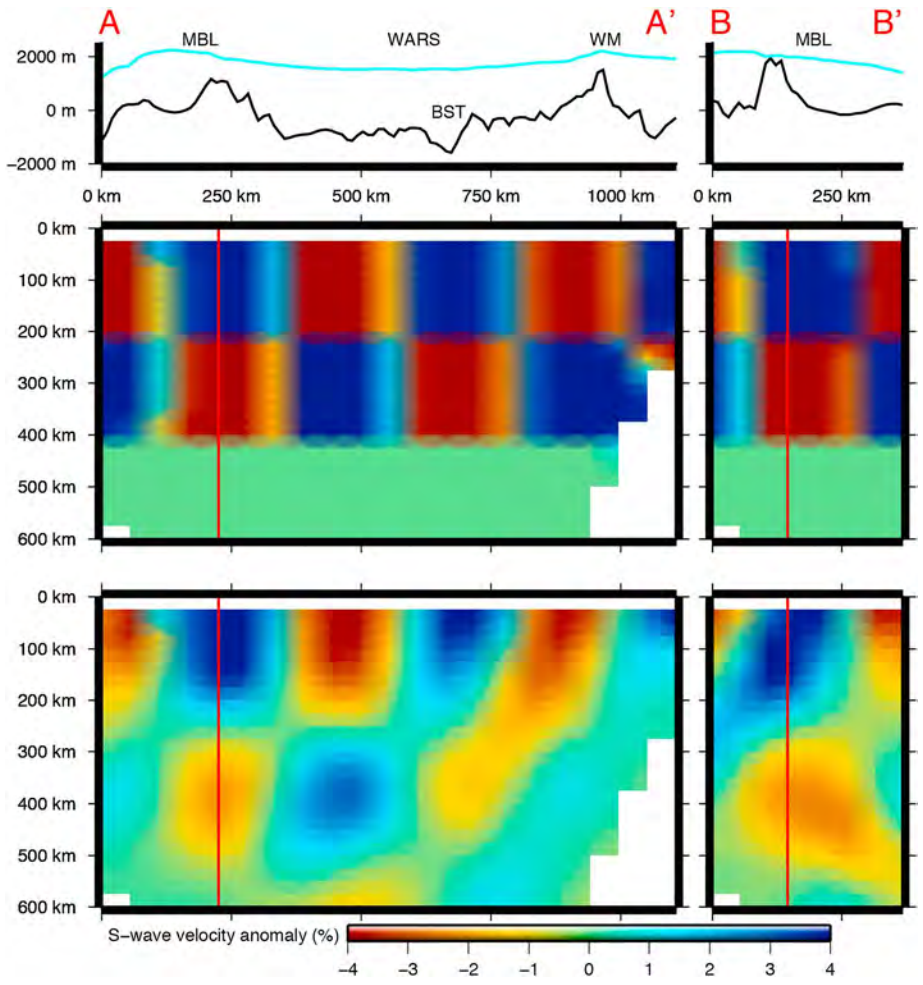

Figure 8. Vertical slices through an *S* wave resolution test consisting of two layers of alternating checkers. The (top) input and (bottom) output are shown for profiles A-A′ and B-B′, whose location is shown in Figures 7a and 7b. The vertical red line indicates the intersection of A-A′ and B-B′. Abbreviations are as follows: MBL, Marie Byrd Land; WARS, West Antarctic Rift System; BST, Bentley Subglacial Trench; WM, Whitmore Mountains.

velocities beneath the Bentley Subglacial Trench extend for ~100 km to the southern flank of the trench. Third, from the south of the Bentley Subglacial Trench to the southern limit of the model, *P* and *S* wave velocities become notably faster than the mean of the models ($\delta V_p > 1.0\%$ and $\delta V_s > 2.0\%$), extending into the Ellsworth-Whitmore mountains crustal block as defined by *Dalziel and Elliot* [1982].

Upper mantle *P* and *S* positive velocity anomalies beneath the Ellsworth-Whitmore mountains crustal block range from ~0% to ~2% and ~1% to ~4%, respectively. Here the fastest velocities ($\delta V_p > 1.0\%$ and $\delta V_s > 2.0\%$) for both models are observed north and south of the Whitmore Mountains and extend down to ~200 km depth (Figures 9–12), but due to limited vertical resolution smear by at least 100 km (Figures 6 and 8). The upper mantle directly beneath the Whitmore Mountains is seismically slower ($\delta V_p \approx 0\%$ and $\delta V_s \approx 1.0\%$). The lateral extent of these anomalies is poorly constrained to the geographic east, south, and west due to limited resolution.

5. Discussion

The models presented here show relative *P* and *S* wave velocity perturbations, as they are derived from relative travel time residuals, and therefore, the anomalies are relative to the average velocity structure of the study region as sampled by the network. Constraints on the average velocity structure can be obtained from absolute shear wave velocity models [e.g., *An et al.*, 2015; D. S. Heeszel et al., submitted manuscript, 2015].

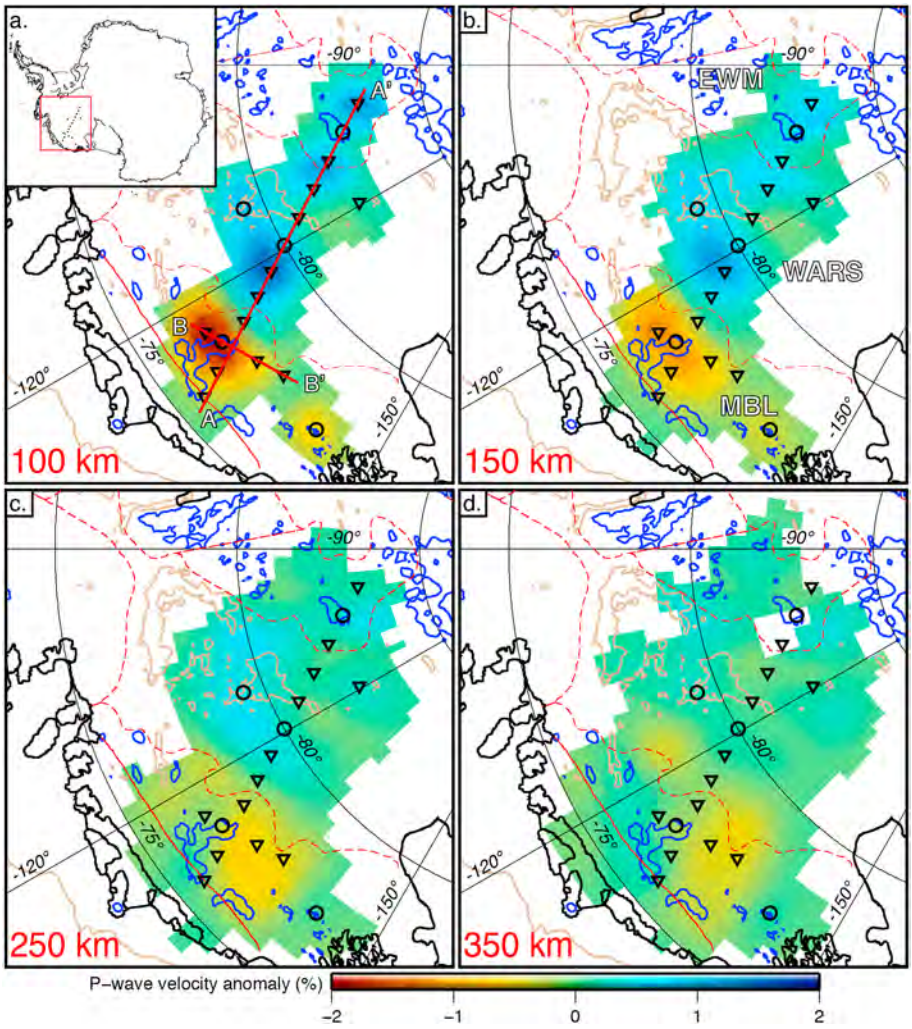

Figure 9. Horizontal slices through the *P* wave tomography model at depths of 100, 150, 250, and 350 km. Each horizontal slice shows the −1500 m (tan) and 800 m (blue) contour from BEDMAP2 [*Fretwell et al.*, 2013]. Abbreviations are as follows: MBL, Marie Byrd Land; WARS, West Antarctic Rift System; EWM, Ellsworth-Whitmore mountains crustal block.

For example, the surface wave study of D. S. Heeszel et al. (submitted manuscript, 2015) indicates that vertically polarized shear wave velocities, V_{SV}, beneath our study region range from 4.20 to 4.46 km/s between 50 and 150 km depth. At these depths, after correcting the AK135 global reference Earth model [*Kennett et al.*, 1995] for the ~4% radial anisotropy (i.e., $(V_{SH} - V_{SV})/V_{SV}$) observed in the uppermost mantle of West Antarctica [*Ritzwoller et al.*, 2001], the global average V_{SV} is ~4.41 km/s. This indicates that the faster shear wave velocities in the uppermost mantle are near the global average, while most are slower and are inferred to indicate regionally elevated upper mantle temperatures, consistent with continental-scale tomographic studies [*Roult et al.*, 1994; *Danesi and Morelli*, 2001; *Ritzwoller et al.*, 2001; *Sieminski et al.*, 2003; *An et al.*, 2015].

Our *P* and *S* relative travel time residuals (Figure 3) can be usefully compared to *P* and *S* station-side delay times within North America, which are derived from crust-corrected absolute delay times [*Lou and van der Lee*, 2014]. Similar to the uppermost mantle of West Antarctica, slow V_{SV} values near 4.2 km/s are observed beneath the Western U.S. (e.g., Basin and Range), while velocities between 4.4 and 4.5 km/s are observed beneath portions of the Great Plains [*Shen et al.*, 2013]. Delay times that are predominantly sensitive to upper mantle structure for both *P* and *S* phases across these regions have a range of ~2 s and ~6 s, respectively, with the most advanced arrivals being near the North American average [*Lou and van der Lee*, 2014]. This range is comparable to *P* and *S* relative travel time residuals in West Antarctica (Figure 3), suggesting that the level of

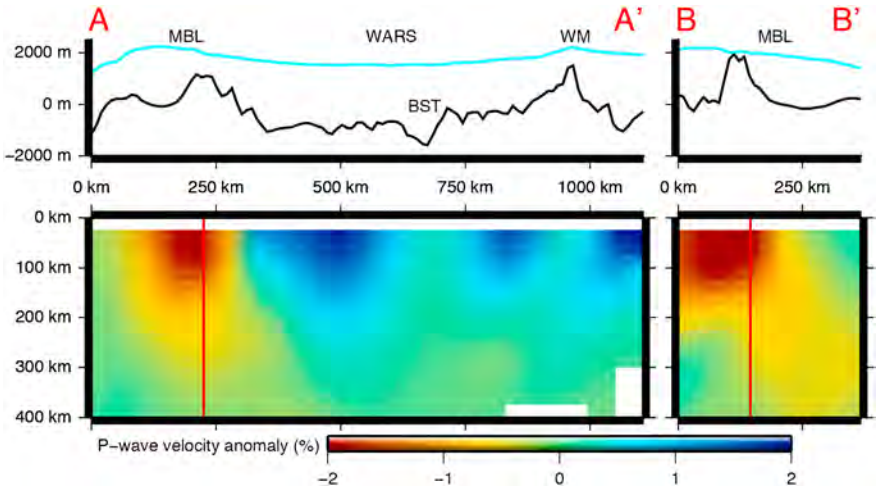

Figure 10. Vertical slices through the *P* wave tomography model along profile A-A′ and B-B′. Each vertical slice shows the bedrock (black) and surface (cyan) topography [*Fretwell et al*., 2013] along the profiles shown in Figure 9a. The vertical red line indicates the intersection of A-A′ and B-B′. Abbreviations are as follows: MBL, Marie Byrd Land; WARS, West Antarctic Rift System; BST, Bentley Subglacial Trench; WM, Whitmore Mountains.

seismic heterogeneity beneath our study region is broadly comparable to that across the much more densely sampled and more extensively studied Western U.S. and portions of the Great Plains.

In the following subsections we discuss both the relative *P* and *S* wave velocity models and their implications for the lithospheric structure of the Ellsworth-Whitmore mountains crustal block, the possibility of recent extension within the eastern WARS, and the source of Cenozoic volcanism and topographic support of MBL.

5.1. Lithospheric Structure of the Ellsworth-Whitmore Mountains Crustal Block

The station residual maps (Figure 3) and tomographic images (Figures 9–12) indicate that fast relative *P* wave velocities and the fastest relative *S* wave velocities in the study region are in the vicinity of the Ellsworth-Whitmore mountains crustal block. Specifically, the fastest velocities in this region are observed north and south of the Whitmore Mountains and extend to the southern boundary of the Bentley Subglacial Trench. The fast velocities in the vicinity of the Whitmore Mountains show large-amplitude lateral variability, suggesting the existence of small-scale heterogeneity within the Ellsworth-Whitmore mountains crustal block. This heterogeneity is more prominent in the *P* wave residual map (Figure 3a) and may be due to differences in V_p/V_s within the Ellsworth-Whitmore mountains crustal block or the higher frequencies at which the *P* wave relative travel time residuals are measured. In the case of the latter, the higher-frequency (0.4–2.0 Hz) *P* phase arrivals have a narrower sensitivity kernel than the lower frequency (0.04–0.2 Hz) *S* phase arrivals, and thus, the *P* wave relative travel time residuals are accumulated over a smaller volume allowing for finer spatial resolution. Resolution tests (Figures 6 and 8) suggest that the fast relative velocity anomalies are consistent with this structure being confined to the upper 100 km of the mantle. This implies that the lithosphere south of the Bentley Subglacial Trench and beneath the Ellsworth-Whitmore mountains crustal block has a different character than the rest of the study region.

The inferred position of the Ellsworth-Whitmore mountains crustal block within Gondwanaland [*Schopf*, 1969; *Grunow et al*., 1987; *Randall and Mac Niocaill*, 2004] and the underlying Precambrian basement observed in the outcrop geology [*Millar and Pankhurst*, 1987] permits the possibility of a Precambrian keel for this region. Globally, unmodified Precambrian lithosphere typically ranges in thickness from >200 km to as thin as ~100 km [*Artemieva and Mooney*, 2001] with shear wave velocities in excess of 2–3% above the global average [*Lebedev et al*., 2009]. In our model the fastest shear wave velocities, 3–4% relative to the mean of the model, at most map to 1–2% faster than the global average. In addition, our inferred thickness of the fast velocities, ~100 km, in both the *P* and *S* body wave tomography is consistent with ~80 km thick lithosphere, as suggested by the vertically polarized shear wave velocity model of D. S. Heeszel et al. (submitted manuscript, 2015). Although shear wave velocities may be faster than the global average south of the Bentely Subglacial Trench, they are too slow and the inferred lithospheric thickness is too thin to typify unmodified

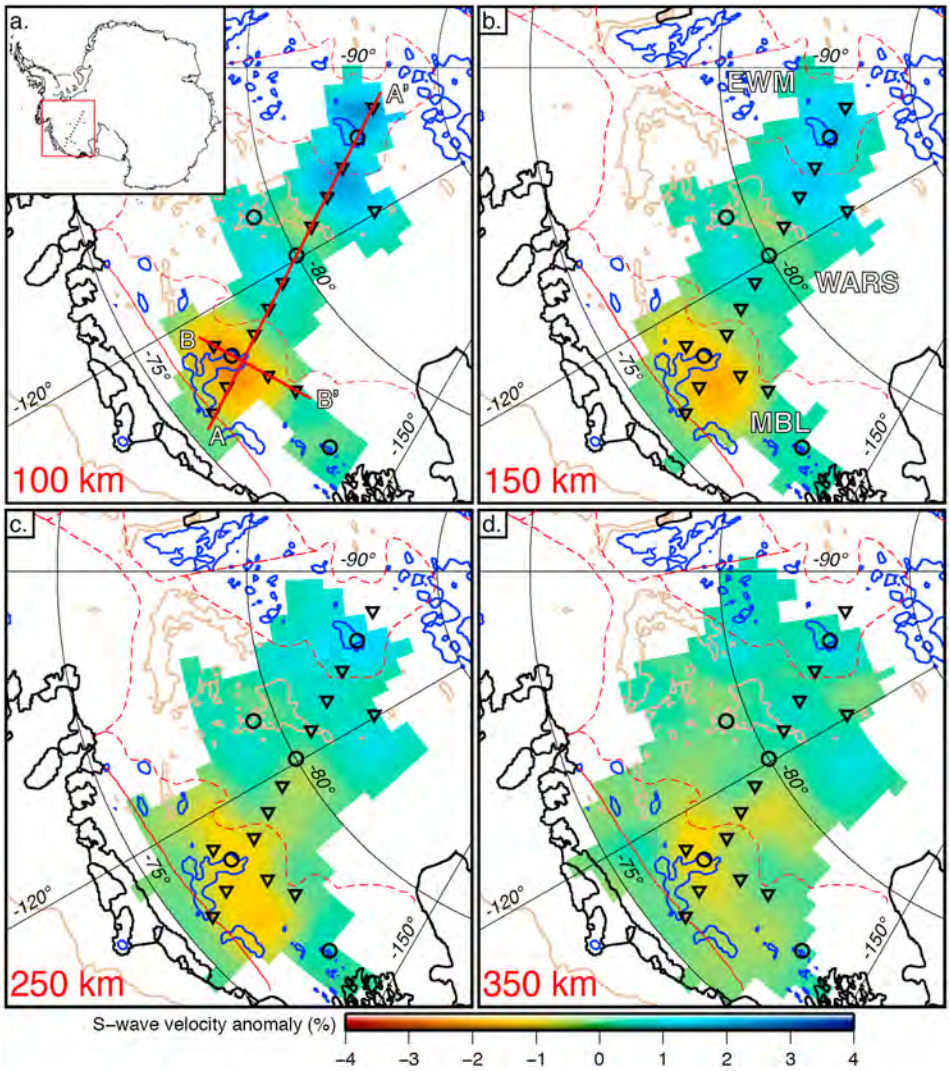

Figure 11. Horizontal slices through the *S* wave tomography model at depths of 100, 150, 250, and 350 km. Each horizontal slice shows the −1500 m (tan) and 800 m (blue) contour from BEDMAP2 [*Fretwell et al.*, 2013]. Abbreviations are as follows: MBL, Marie Byrd Land; WARS, West Antarctic Rift System; EWM, Ellsworth-Whitmore mountains crustal block.

Precambrian lithosphere. Instead, we propose that the lithosphere in this region is a product of both thermal and chemical modification, as well as delamination since the Jurassic in response to the breakup of Gondwanaland, the emplacement of mid-Jurassic within-plate granites, and the subsequent development of the WARS. Modification of Precambrian lithospheric mantle is not uncommon and is observed beneath the North China Craton [*Fan et al.*, 2000], beneath the Hebridean and other Precambrian terranes of Northwest Scotland [*Menzies and Halliday*, 1988], and in western North America [e.g., *Van Wijk et al.*, 2010].

The relative fast seismic velocities south of the Bentley Subglacial Trench and beneath the Ellsworth-Whitmore mountains crustal block stand in stark contrast to a proposed active subglacial volcano, near ST02 (82° 52.6'S, 111° 18.1'W; Figure 1), inferred from aerogeophysical observations that report a high magnetic anomaly (600 nT) centered on a 6 km wide peak in the bedrock topography [*Blankenship et al.*, 1993]. If this topographic feature is indeed a recently active subglacial volcano, then the imaged *P* and *S* wave velocities beneath the region are expected to be slower, perhaps not unlike those observed beneath the Executive Committee Range in MBL (Figures 9–12), which has a deep active magmatic system [*Lough et al.*, 2013]. Instead, the uppermost mantle velocities are indicative of stable lithospheric conditions and provide no evidence of a comparable thermal anomaly that would accompany an active volcano. Other magnetic anomalies associated with sub-ice topographic highs are also observed in the area and throughout the WARS, and have been inferred to be late

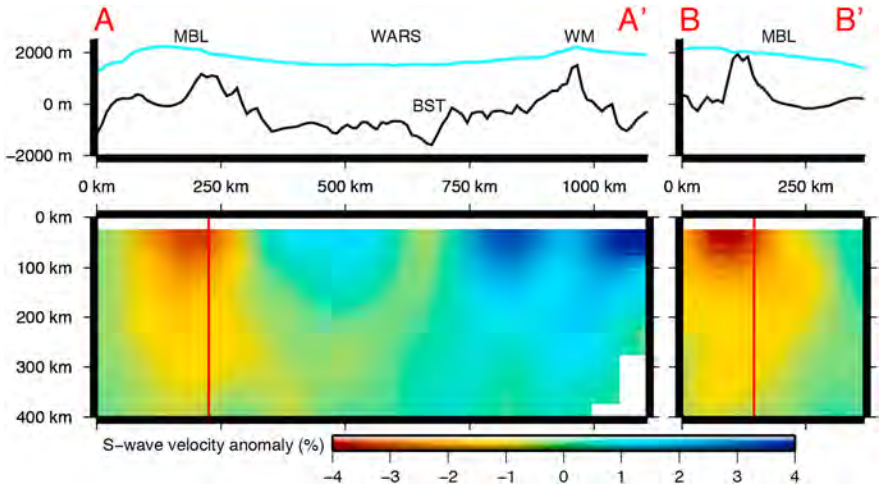

Figure 12. Vertical slices through the *S* wave tomography model along profile A-A′ and B-B′. Each vertical slice shows the bedrock (black) and surface (cyan) topography [*Fretwell et al.*, 2013] along the profiles shown in Figure 11a. The vertical red line indicates the intersection of A-A′ and B-B′. Abbreviations are as follows: MBL, Marie Byrd Land; WARS, West Antarctic Rift System; BST, Bentley Subglacial Trench; WM, Whitmore Mountains.

Cenozoic in age [e.g., *Behrendt*, 1999]. One such anomaly, near station WNDY (Figure 1), is underlain by high resistivity in both the crust and uppermost mantle, which is consistent with fluid-poor conditions in the crust and quiescent stable lithosphere [*Wannamaker et al.*, 1996]. These observations not only preclude active volcanism south of the Bentley Subglacial Trench in the study region, but also suggest that the inferred sub-ice volcanic structures are older (perhaps Late Cretaceous/early Cenozoic).

5.2. A Mantle Thermal Anomaly Beneath the Bentley Subglacial Trench

Much of the uppermost mantle seismic structure of the WARS imaged in this study is dominated by fast relative *P* and *S* wave velocities with the notable exception of the Bentley Subglacial Trench, which is underlain by relative *P* and *S* wave velocities near the model mean (Figures 9–12). Velocity anomalies within the WARS are spatially consistent between the two tomographic models, and resolution tests indicate that they are laterally well resolved (Figures 5–8). The slower uppermost mantle velocities of the Bentley Subglacial Trench also coincide with deep bedrock topography, ~2.5 km below sea level (prior to correcting for the ice sheet load), and locally thinned crust, ~19 km thick, [*Winberry and Anandakrishnan*, 2004; *Jordan et al.*, 2010; *Chaput et al.*, 2014]. These attributes are indicative of a region that has thinned in a ductile manner under pure shear extension due to thermal weakening and or along a preexisting basement weakness [e.g., *Wilson et al.*, 2005]. Inferred focused narrow extension within the Bentley Subglacial Trench and other similar subglacial basins (e.g., Byrd Subglacial Basin) has, by analogy to the Ross Sea sector of the WARS, been suggested to have occurred during the Neogene [*LeMasurier*, 2008; *Jordan et al.*, 2010; *Bingham et al.*, 2012], distinct from broad distributed extension characterizing the Late Cretaceous/early Cenozoic [e.g., *Luyendyk*, 1995; *Wilson and Luyendyk*, 2009].

The predominance of temperature in controlling lateral variations of seismic velocities in the upper mantle in the absence of prominent chemical heterogeneity [e.g., *Karato*, 1993; *Faul and Jackson*, 2005] allows us to infer that the narrow region of slower velocities, near the model mean, beneath the Bentley Subglacial Trench may reflect a recent phase of extension within West Antarctica. Conversely, fast relative velocities beneath the remainder of the WARS may reflect zones of Late Cretaceous/early Cenozoic extension whose thermal perturbation due to rifting has largely dissipated. Assuming $\partial V_s/\partial T$ is $1.2\,\mathrm{m\,s^{-1}\,K^{-1}}$ [*Faul and Jackson*, 2005; *Wiens et al.*, 2008], then the 2.0% difference in *S* wave velocities (which may be underrecovered due to resolution limitations) is consistent with an ~75 K difference in temperature. Given this temperature difference and constraints on the lithospheric structure [*Chaput et al.*, 2014; D. S. Heeszel et al., submitted manuscript, 2015], a simple model for the thermal evolution of a rift basin [*McKenzie*, 1978, equation (5)] may provide further constraints on the timing of extension within the Bentley Subglacial Trench.

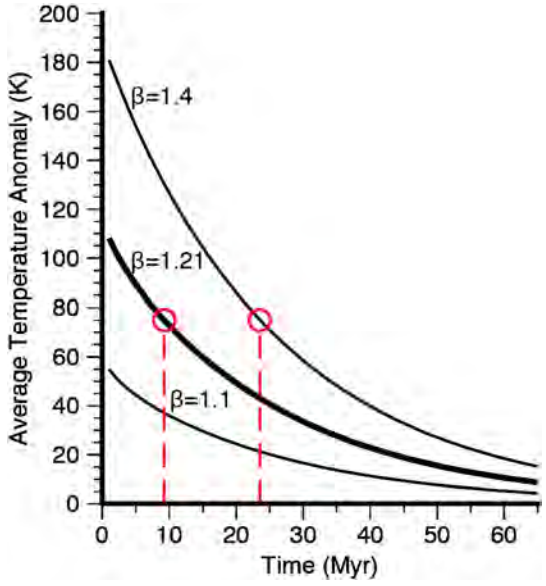

Figure 13. Following *McKenzie* [1978], models for the evolution of the average temperature anomaly beneath the BST relative to the rest of the WARS. Results are shown for a range of stretching factors, β, which reflects the error in crustal thickness measurements. Open red circles indicate the uppermost mantle temperature difference between the BST and the rest of the WARS inferred from our *S* wave velocity model.

Following *McKenzie* [1978], the thermal evolution of the Bentley Subglacial Trench is modeled assuming a starting structure similar to those regions of the WARS where fast relative seismic velocities are observed, as such the initial lithospheric and crustal thickness is taken to be 80 km (D. S. Heeszel et al., submitted manuscript, 2015) and 23 km [*Chaput et al.*, 2014], respectively. The stretching factor, $\beta = 1.21$, is determined assuming a final crustal thickness of 19 km within the Bentley Subglacial Trench [*Winberry and Anandakrishnan*, 2004; *Chaput et al.*, 2014]. However, a range of stretching factors between 1.1 and 1.4 are explored in order to account for errors associated with the crustal thickness measurements. At each time step the average temperature anomaly is computed relative to an initial conductive geotherm with boundary conditions of 0°C and 1333°C at the top and bottom of the lithosphere, respectively. The evolution of the average temperature anomaly of the Bentley Subglacial Trench (Figure 13) suggests that the 75 K thermal anomaly inferred from our *S* wave velocity model is consistent with extension during the Neogene.

The lack of any geological data from the Bentley Subglacial Trench makes it natural to seek a well-studied rift showing similar geophysical characteristics. The Rio Grande Rift may represent a reasonable analog, having undergone several episodes of rifting, with the most recent between 5 and 10 Ma [*Chapin and Cather*, 1994], with very low and broadly distributed rates of the present-day extensional strain [*Berglund et al.*, 2012] and low rift-related seismicity rates [e.g., *Keller et al.*, 1991]. Nonetheless, despite the lack of current tectonic motion and seismicity, the rift shows prominent volcanism, a significant seismic anomaly indicative of high upper mantle temperatures [*Wilson et al.*, 2005], and scattered elevated heat flow ranging from 70 to 150 mW/m^2 [*Morgan et al.*, 1986]. Similar elevated heat flow may exist within the Bentley Subglacial Trench region due to recent extension inferred from the shear wave structure in the uppermost mantle within the WARS (Figures 11 and 12). This is consistent with anomalously high heat flow reported at the West Antarctic Ice Sheet Divide Ice Core [*Clow et al.*, 2012] and at Subglacial Lake Whillans [*Fisher et al.*, 2015], both of which are spatially close to the Bentley Subglacial Trench. Elevated heat flow has also been reported for the Thwaites Glacier catchment [*Schroeder et al.*, 2014], which comprises a large portion of the Byrd Subglacial Basin in the eastern WARS. Despite these intriguing recent studies, heat flow is still poorly constrained across Antarctica and remains one of the largest uncertainties in ice flow models [*Larour et al.*, 2012].

5.3. Source of Cenozoic Volcanism and Uplift of Marie Byrd Land

The slowest and one of the most prominent anomalies in both the relative *P* and *S* wave velocity models appears beneath eastern MBL, centered near Mount Sidley in the Executive Committee Range (Figures 9–12) and is observed extending to ~200 km depth. Along the strike of this linear volcanic chain, near ST08 (Figure 1), seismicity characteristic of magma migration within the lower crust indicates an active magmatic system [*Lough et al.*, 2013]. At depths shallower than 200 km both *P* and *S* wave velocities beneath other resolved portions of MBL are nearer the model mean, which is reflected in the station residual maps (Figure 3). The pattern of the slow velocity anomalies beneath MBL correlates well with long-wavelength elevated topography [*Chaput et al.*, 2014] that, in concert with an active magmatism, suggests both the high elevation and volcanism result from an upper mantle thermal anomaly.

Using mantle temperature anomalies computed from the relative shear wave velocities (Figures 11 and 12) and constraints on the crustal structure of MBL and the WARS [*Chaput et al.*, 2014], the expected difference in topography between the two regions can be estimated with a simple isostatic equilibrium calculation. In this instance, both MBL and the surrounding WARS region are modeled as two layers consisting of a crust of identical density ($\rho_c = 2750\ \mathrm{kg/m^3}$) overlying a mantle layer with a reference density (ρ_m) of $3250\ \mathrm{kg/m^3}$. However, the mantle beneath MBL is assumed to contain a region of anomalous density (ρ_a) with a thickness t_a. The isostatic equilibrium equation is then

$$t_{\mathrm{mbl}}\rho_c + t_a\rho_a = t_{\mathrm{wars}}\rho_c + (t_{\mathrm{mbl}} + t_a - t_{\mathrm{wars}} - h)\rho_m, \tag{3}$$

where t_{mbl} and t_{wars} are the average crustal thicknesses of MBL and the WARS and h is the difference in average topography between the two regions. Solving for the topography difference, h, gives

$$h = [(t_{\mathrm{mbl}} - t_{\mathrm{wars}})(\rho_m - \rho_c) + t_a(\rho_m - \rho_a)]\rho_m^{-1}. \tag{4}$$

Values for t_{mbl} and t_{wars} are constrained by receiver function results to be 28.5 km and 23 km, respectively [*Chaput et al.*, 2014]. Constraints for t_a and ρ_a can be gleaned from our relative shear wave velocity model (Figures 11 and 12). The MBL anomaly, defined as the region where $\delta V_s < -2.0\%$, is observed extending to ~200 km, and resolution tests indicate at least 50 km of vertical smearing. This implies a thickness, t_a, of ~120 km. An average difference in shear wave velocity of ~4.0% (which could be underestimated based on limited resolution) is observed between the MBL anomaly and the juxtaposed faster velocities of the WARS. Assuming $\partial V_s/\partial T$ is $1.2\ \mathrm{m\,s^{-1}\,K^{-1}}$ [*Faul and Jackson*, 2005; *Wiens et al.*, 2008] and a thermal expansion coefficient of $3.4 \times 10^{-5}\ \mathrm{K^{-1}}$ [*Afonso et al.*, 2005], a 4.0% change in shear wave velocity corresponds to a temperature difference of ~150 K and a density anomaly, $\rho_m - \rho_a$, of ~17 kg/m^3. Using these values the expected difference in topography between MBL and the adjacent WARS is ~1.5 km, which is similar to the observed peak difference in the long-wavelength deglaciated bedrock topography (~1.25 km) [*Chaput et al.*, 2014]. Thus, the magnitude and thickness of the observed seismic anomaly suggest that the MBL topography is indeed supported by an upper mantle thermal anomaly with a temperature contrast of ~150 K with the surrounding region.

The deeper structure and ultimate origin of the inferred upper mantle thermal anomaly imaged in both the *P* and *S* wave tomographic models is poorly constrained. Upper mantle thermal anomalies may be linked to mantle plumes originating in the deep mantle, in which geodynamical models of classical mantle plumes generally show a widespread "head" impinging beneath the lithosphere that is fed by a thin conduit extending from a thermal boundary layer [*Campbell and Griffiths*, 1990; *Sleep*, 1990]. However, recent global and regional tomography suggest that convective connectivity between the base and the top of the mantle does not have this geometry and is instead considerably broader and more disrupted [e.g., *Schmandt et al.*, 2012; *French and Romanowicz*, 2015]. It is possible that a thin conduit below the MBL anomaly could go undetected in our models; however, transition zone receiver functions do not indicate a mantle thermal anomaly beneath this region of MBL at transition zone depths [*Emry et al.*, 2015]. Transition zone thinning, indicative of elevated mantle temperatures, is observed elsewhere in West Antarctica with the most significant beneath the MBL coast geographically northwest of station CLRK (Figure 1), and thinning is also noted to a lesser extent beneath the Whitmore Mountains and the Bentley Subglacial Trench [*Emry et al.*, 2015].

6. Summary and Conclusions

Teleseismic *P* and *S* wave arrivals recorded by a subset of POLENET/A-NET broadband seismic stations deployed in a transect across central West Antarctica between January 2010 and January 2012 have been used to develop independent regional *P* and *S* wave relative velocity models. The resolution of both models was evaluated through a series of synthetic checkerboard tests (e.g., Figures 5–8), which indicate that horizontal anomalies at least ~100 km and ~ 200 km wide are well resolved to 200 km and 400 km depth, respectively. Vertical resolution is poorer with anomalies smearing vertically by at least 50 km in the most well-resolved regions to more than 100 km in the least well-resolved regions. At these length scales the minimum difference in velocity (δV_p and δV_s) that can be resolved is ~0.3% and ~0.6%, respectively. However, model velocity variations may underrepresent true variations due to limited resolution.

Modeled seismic heterogeneity across the study region is substantially confined to the upper 200 km of the mantle and loosely correlates with the major West Antarctic crustal blocks comprising the study region

(Figures 9–12). In addition, prominent bedrock features, such as the Bentley Subglacial Trench, are found to be seismically distinct in the upper most portion of the mantle. Below 200 km depth the upper mantle is largely homogenous or unresolved.

Within the upper half of the tomographic images (Figures 9–12) distinct lithospheric mantle, likely faster than the global average, underlies the Ellsworth-Whitmore mountains crustal block and extends to the southern boundary of the Bentley Subglacial Trench. Despite the basement of the Ellsworth-Whitmore mountains crustal block being Precambrian, the underlying mantle lithosphere is too slow and too thin to be characteristic of an unmodified Precambrian keel. Instead, the lithosphere in this region has likely been thermally, chemically, and structurally modified since the breakup of Gondwanaland. Structure within the WARS is dominated by Late Cretaceous/early Cenozoic extension as inferred from the fast relative seismic velocities; thus, little rift related heat flow is expected. However, slower relative seismic velocities in the uppermost mantle beneath the Bentley Subglacial Trench when compared with thermal evolution models for a rift basin suggest extension occurred during the Neogene (Figure 13). Recent extension in the Bentley Subglacial Trench may in part account for elevated heat flow reported at the nearby West Antarctic Ice Sheet Divide Ice Core [*Clow et al*., 2012] and at Subglacial Lake Whillans [*Fisher et al*., 2015]. The slowest and most prominent anomaly for both *P* and *S* waves is observed beneath the Executive Committee Range in MBL. This slow-velocity anomaly is inferred to be an upper mantle thermal anomaly that is sufficient to support isostatically the anomalously high long-wavelength topography of MBL. Although this feature is prominent and distinct within the upper mantle, it is difficult to rule out a plume model due to limited deeper resolution.

Acknowledgments

We wish to thank IRIS-PASSCAL Polar for providing field support during the installation and continued upkeep of the POLENET/A-NET array in Antarctica, as well as the pilots and staff of Kenn Borek Air and the New York Air National Guard for flight support. We thank all individuals that have aided and contributed to the success of POLENET/A-NET project. We also thank Anya Reading and an anonymous reviewer for their helpful critiques on this manuscript. POLENET/A-NET was supported by United States National Sciences Foundation (NSF) grants ANT-0632230, 0632239, 0652322, 0632335, 0632136, 0632209, and 0632185. Additionally, this research was funded by contract 1514454 provided by NASA Science Mission Directorate Award NNH13ZDA001N 13-SLR13-0004 (Sea Level Rise). Seismic instrumentation provided and supported by the Incorporated Research Institutions for Seismology (IRIS) through the PASSCAL Instrument Center at New Mexico Tech. Data are available through the IRIS Data Management Center. The facilities of the IRIS Consortium are supported by the National Science Foundation under cooperative agreement EAR-1063471, the NSF Office of Polar Programs, and the DOE National Nuclear Security Administration. Additional information regarding the POLENET/A-NET project, sites, and data are available at http://polenet.org. Figures in this paper were created using GMT [*Wessel and Smith*, 1998].

References

A, G., J. Wahr, and S. Zhong (2013), Computations of the viscoelastic response of a 3-D compressible Earth to surface loading: An application to glacial isostatic adjustment in Antarctica and Canada, *Geophys. J. Int.*, *192*, 557–572.

Afonso, J. C., G. Ranalli, and M. Fernàndez (2005), Thermal expansivity and elastic properties of the lithospheric mantle: Results from mineral physics of composites, *Phys. Earth Planet. Inter.*, *149*(3), 279–306.

Aki, K., and W. H. K. Lee (1976), Determination of three-dimensional velocity anomalies under a seismic array using first *P* arrival times from local earthquakes: 1. A homogeneous initial model, *J. Geophys. Res.*, *81*(23), 4381–4399.

Alley, R. B. (1989), Water-pressure coupling of sliding and bed deformation: I. Water system, *J. Glaciol.*, *35*(119), 108–118.

An, M., D. A. Wiens, Y. Zhao, M. Feng, A. A. Nyblade, M. Kanao, Y. Li, A. Maggi, and J. J. Lévêque (2015), *S*-velocity model and inferred Moho topography beneath the Antarctic Plate from Rayleigh waves, *J. Geophys. Res. Solid Earth*, *120*, 359–383, doi:10.1002/2014JB011332.

Artemieva, I. M., and W. D. Mooney (2001), Thermal thickness and evolution of Precambrian lithosphere: A global study, *J. Geophys. Res.*, *106*(B8), 16,387–16,414.

Behrendt, J. C. (1999), Crustal and lithospheric structure of the West Antarctic Rift System from geophysical investigations—A review, *Global Planet. Change*, *23*(1), 25–44.

Behrendt, J. C., W. E. LeMasurier, A. K. Cooper, F. Tessensohn, A. Trehu, and D. Damaske (1991), Geophysical studies of the West Antarctic rift system, *Tectonics*, *10*(6), 1257–1273.

Berglund, H., A. Sheehan, M. Murray, M. Roy, A. Lowry, R. Nerem, and F. Blume (2012), Distributed deformation across the Rio Grande Rift, Great Plains, and Colorado Plateau, *Geology*, *40*, 23–26.

Bingham, R. G., F. Ferraccioli, E. C. King, R. D. Larter, H. D. Pritchard, A. M. Smith, and D. G. Vaughan (2012), Inland thinning of West Antarctic Ice Sheet steered along subglacial rifts, *Nature*, *487*(7408), 468–471.

Blankenship, D. D., R. E. Bell, S. M. Hodge, J. M. Brozena, J. C. Behrendt, and C. A. Finn (1993), Active volcanism beneath the West Antarctic ice sheet and implications for ice-sheet stability, *Nature*, *361*, 526–529.

Block, A. E., R. E. Bell, and M. Studinger (2009), Antarctic crustal thickness from satellite gravity: Implications for the Transantarctic and Gamburtsev Subglacial Mountains, *Earth Planet. Sci. Lett.*, *288*(1), 194–203.

Campbell, I. H., and R. W. Griffiths (1990), Implications of mantle plume structure for the evolution of flood basalts, *Earth Planet. Sci. Lett.*, *99*, 79–93.

Cande, S. C., and J. M. Stock (2004), Cenozoic reconstructions of the Australia-New Zealand-South Pacific sector of Antarctica, in *The Cenozoic Southern Ocean: Tectonics, Sedimentation, and Climate Change Between Australia and Antarctica*, pp. 5–17, AGU, Washington, D. C.

Chapin, C. E., and S. M. Cather (1994), Tectonic setting of the axial basins of the northern and central Rio Grande rift, *Geol. Soc. Am. Spec. Pap.*, *291*, 5–26.

Chaput, J., R. C. Aster, A. Huerta, X. Sun, A. Lloyd, D. Wiens, A. Nyblade, S. Anandakrishnan, J. P. Winberry, and T. Wilson (2014), The crustal thickness of West Antarctica, *J. Geophys. Res. Solid Earth*, *119*, 378–395, doi:10.1002/2013JB010642.

Clow, G. D., K. M. Cuffey, and E. D. Waddington (2012), High heat-flow beneath the central portion of the West Antarctic ice sheet, in AGU Fall Meeting Abstracts, vol. 1, p. 0577.

Dalziel, I. W. D., and D. H. Elliot (1982), West Antarctica: Problem child of Gondwanaland, *Tectonics*, *1*(1), 3–19.

Dalziel, I. W., L. A. Lawver, I. O. Norton, and L. M. Gahagan (2013), The Scotia Arc: Genesis, evolution, global significance, *Annu. Rev. Earth Planet. Sci.*, *41*, 767–793.

Danesi, S., and A. Morelli (2001), Structure of the upper mantle under the Antarctic Plate from surface wave tomography, *Geophys. Res. Lett.*, *28*(23), 4395–4398.

DeConto, R. M., and D. Pollard (2003), A coupled climate–ice sheet modeling approach to the early Cenozoic history of the Antarctic ice sheet, *Palaeogeogr. Palaeoclimatol. Palaeoecol.*, *198*(1), 39–52.

Donnellan, A., and B. P. Luyendyk (2004), GPS evidence for a coherent Antarctic plate and for postglacial rebound in Marie Byrd Land, *Global Planet. Change*, *42*(1), 305–311.

Elliot, D. H., and T. H. Fleming (2004), Occurrence and dispersal of magmas in the Jurassic Ferrar large igneous province, Antarctica, *Gondwana Res.*, *7*(1), 223–237.
Emry, E. L., A. A. Nyblade, J. Julià, S. Anandakrishnan, R. C. Aster, D. A. Wiens, A. D. Huerta, and T. J. Wilson (2015), The mantle transition zone beneath West Antarctica: Seismic evidence for hydration and thermal upwellings, *Geochem. Geophys. Geosyst.*, *16*, 40–58, doi:10.1002/2014GC005588.
Evison, F. F., C. E. Ingham, R. A. Orr, and L. H. Le Fort (1960), Thickness of the Earth's crust in Antarctica and the surrounding oceans, *Geophys. J. Int.*, *3*(3), 289–306.
Fan, W. M., H. F. Zhang, J. Baker, K. E. Jarvis, P. R. D. Mason, and M. A. Menzies (2000), On and off the North China Craton: Where is the Archaean keel?, *J. Petrol.*, *41*(7), 933–950.
Faul, U. H., and I. Jackson (2005), The seismological signature of temperature and grain size variations in the upper mantle, *Earth Planet. Sci. Lett.*, *234*(1), 119–134.
Fielding, C. R., J. Whittaker, S. A. Henrys, T. J. Wilson, and T. R. Naish (2008), Seismic facies and stratigraphy of the Cenozoic succession in McMurdo Sound, Antarctica: Implications for tectonic, climatic and glacial history, *Palaeogeogr. Palaeoclimatol. Palaeoecol.*, *260*(1), 8–29.
Finn, C. A., R. D. Müller, and K. S. Panter (2005), A Cenozoic diffuse alkaline magmatic province (DAMP) in the southwest Pacific without rift or plume origin, *Geochem. Geophys. Geosyst.*, *6*, Q02005, doi:10.1029/2004GC000723.
Fisher, A. T., K. D. Mankoff, S. M. Tulaczyk, S. W. Tyler, and N. Foley (2015), High geothermal heat flux measured below the West Antarctic Ice Sheet, *Sci. Adv.*, *1*(6), e1500093, doi:10.1126/sciadv.1500093.
French, S. W., and B. Romanowicz (2015), Broad plumes rooted at the base of the Earth's mantle beneath major hotspots, *Nature*, *525*, 95–99.
Fretwell, P., et al. (2013), Bedmap2: Improved ice bed, surface and thickness datasets for Antarctica, *Cryosphere*, *7*(1), 375–393.
Granot, R., S. C. Cande, J. M. Stock, F. J. Davey, and R. W. Clayton (2010), Postspreading rifting in the Adare Basin, Antarctica: Regional tectonic consequences, *Geochem. Geophys. Geosyst.*, *11*, Q08005, doi:10.1029/2010GC003105.
Granot, R., S. C. Cande, J. M. Stock, and D. Damaske (2013), Revised Eocene-Oligocene kinematics for the West Antarctic rift system, *Geophys. Res. Lett.*, *40*, 279–284, doi:10.1029/2012GL054181.
Grunow, A. M., I. W. D. Dalziel, and D. V. Kent (1987), Ellsworth-Whitmore Mountains Crustal Block Western Antarctica: New paleomagnetic results and their tectonic significance, in *Gondwana Six: Structure, Tectonics, and Geophysics*, pp. 161–171, AGU, Washington, D. C.
Grunow, A. M., D. V. Kent, and I. W. D. Dalziel (1991), New paleomagnetic data from Thurston Island: Implications for the tectonics of West Antarctica and Weddell Sea opening, *J. Geophys. Res.*, *96*(B11), 17,935–17,954.
Hansen, S. E., J. H. Graw, L. M. Kenyon, A. A. Nyblade, D. A. Wiens, R. C. Aster, A. D. Huerta, S. Anandakrishnan, and T. Wilson (2014), Imaging the Antarctic mantle using adaptively parameterized *P*-wave tomography: Evidence for heterogeneous structure beneath West Antarctica, *Earth Planet. Sci. Lett.*, *408*, 66–78.
Henrys, S. A., T. Wilson, C. R. Fielding, J. Hall, and T. R. Naish (2008), Tectonic history of mid-Miocene to present southern Victoria Land Basin, inferred from seismic statigraphy in McMurdo Sound, Antarctica, *Papers in the Earth and Atmospheric Sciences* Paper 285.
Ivins, E. R., and T. S. James (2005), Antarctic glacial isostatic adjustment: A new assessment, *Antarct. Sci.*, *17*(04), 541–553.
Jordan, T. A., F. Ferraccioli, D. G. Vaughan, J. W. Holt, H. Corr, D. D. Blankenship, and T. M. Diehl (2010), Aerogravity evidence for major crustal thinning under the Pine Island Glacier region (West Antarctica), *Geol. Soc. Am. Bull.*, *122*(5–6), 714–726.
Karato, S. I. (1993), Importance of anelasticity in the interpretation of seismic tomography, *Geophys. Res. Lett.*, *20*(15), 1623–1626.
Keller, G. R., M. A. Khan, P. Morganc, R. F. Wendlandt, W. S. Baldridge, K. H. Olsen, C. Prodehl, and L. W. Braile (1991), A comparative study of the Rio Grande and Kenya rifts, *Tectonophysics*, *197*(2), 355–371.
Kennett, B. L. N., and E. R. Engdahl (1991), Traveltimes for global earthquake location and phase identification, *Geophys. J. Int.*, *105*(2), 429–465.
Kennett, B. L. N., E. R. Engdahl, and R. Buland (1995), Constraints on seismic velocities in the Earth from traveltimes, *Geophys. J. Int.*, *122*(1), 108–124.
Larour, E., M. Morlighem, H. Seroussi, J. Schiermeier, and E. Rignot (2012), Ice flow sensitivity to geothermal heat flux of Pine Island Glacier, Antarctica, *J. Geophys. Res.*, *117*, F04023, doi:10.1029/2012JF002371.
Lawrence, J. F., D. A. Wiens, A. A. Nyblade, S. Anandakrishnan, P. J. Shore, and D. Voigt (2006a), Rayleigh wave phase velocity analysis of the Ross Sea, Transantarctic Mountains, and East Antarctica from a temporary seismograph array, *J. Geophys. Res.*, *111*, B06302, doi:10.1029/2005JB00381.
Lawrence, J. F., D. A. Wiens, A. A. Nyblade, S. Anandakrishan, P. J. Shore, and D. Voigt (2006b), Upper mantle thermal variations beneath the Transantarctic Mountains inferred from teleseismic *S*-wave attenuation, *Geophys. Res. Lett.*, *33*, L03303, doi:10.1029/2005GL024516.
Lebedev, S., J. Boonen, and J. Trampert (2009), Seismic structure of Precambrian lithosphere: New constraints from broad-band surface-wave dispersion, *Lithos*, *109*(1), 96–111.
LeMasurier, W. E. (1990), Late Cenozoic volcanism on the Antarctic plate: An overview, in *Volcanoes Antarctic Plate Southern Oceans*, pp. 1–17, AGU, Washington, D. C.
LeMasurier, W. E. (2008), Neogene extension and basin deepening in the West Antarctic rift inferred from comparisons with the East African rift and other analogs, *Geology*, *36*(3), 247–250.
LeMasurier, W. E., and C. A. Landis (1996), Mantle-plume activity recorded by low-relief erosion surfaces in West Antarctica and New Zealand, *Geol. Soc. Am. Bull.*, *108*(11), 1450–1466.
LeMasurier, W. E., and D. C. Rex (1989), Evolution of linear volcanic ranges in Marie Byrd Land, west Antarctica, *J. Geophys. Res.*, *94*(B6), 7223–7236.
Lou, X., and S. van der Lee (2014), Observed and predicted North American teleseismic delay times, *Earth Planet. Sci. Lett.*, *402*, 6–15.
Lough, A. C. (2014), Studies of seismic sources in Antarctica using an extensive deployment of broadband seismographs, PhD thesis, Dep. of Earth and Planet. Sci., Washington Univ. in St Louis, St. Louis, Mo.
Lough, A. C., D. A. Wiens, C. G. Barcheck, S. Anandakrishnan, R. C. Aster, D. D. Blankenship, A. D. Huerta, A. Nyblade, D. A. Young, and T. J. Wilson (2013), Seismic detection of an active subglacial magmatic complex in Marie Byrd Land, Antarctica, *Nat. Geosci.*, *6*, 1031–1035, doi:10.1038/ngeo1992.
Luyendyk, B. P. (1995), Hypothesis for Cretaceous rifting of east Gondwana caused by subducted slab capture, *Geology*, *23*(4), 373–376.
Luyendyk, B., S. Cisowski, C. Smith, S. Richard, and D. Kimbrough (1996), Paleomagnetic study of the northern Ford Ranges, western Marie Byrd Land, West Antarctica: Motion between West and East Antarctica, *Tectonics*, *15*(1), 122–141.
McKenzie, D. (1978), Some remarks on the development of sedimentary basins, *Earth Planet. Sci. Lett.*, *40*(1), 25–32.
Menzies, M., and A. Halliday (1988), Lithospheric mantle domains beneath the Archean and Proterozoic crust of Scotland, *J. Petrol.*, *1*, 275–302.
Millar, I. L., and R. J. Pankhurst (1987), Rb-Sr Geochronology of the region between the Antarctic Peninsula and the Transantarctic Mountains: Haag nunataks and mesozoic granitoids, in *Gondwana Six: Structure, Tectonics, and Geophysics*, pp. 151–160, AGU, Washington, D. C.

Morgan, P., W. R. Seager, and M. P. Golombek (1986), Cenozoic thermal, mechanical and tectonic evolution of the Rio Grande rift, *J. Geophys. Res.*, *91*(B6), 6263–6276.
Mukasa, S. B., and I. W. D. Dalziel (2000), Marie Byrd Land, West Antarctica: Evolution of Gondwana's Pacific margin constrained by zircon U-Pb geochronology and feldspar common-Pb isotopic compositions, *Geol. Soc. Am. Bull.*, *112*(4), 611–627.
Müller, R. D., K. Gohl, S. C. Cande, A. Goncharov, and A. V. Golynsky (2007), Eocene to Miocene geometry of the West Antarctic rift system, *Aust. J. Earth Sci.*, *54*(8), 1033–1045.
O'Donnell, J. P., and A. A. Nyblade (2014), Antarcticas hypsometry and crustal thickness: Implications for the origin of anomalous topography in East Antarctica, *Earth Planet. Sci. Lett.*, *388*, 143–155.
Paige, C. C., and M. A. Saunders (1982), LSQR: An algorithm for sparse linear equations and sparse least squares, *ACM Trans. Math. Software (TOMS)*, *8*(1), 43–71.
Panter, K. S., W. C. McIntosh, and J. L. Smellie (1994), Volcanic history of Mount Sidley, a major alkaline volcano in Marie Byrd Land, Antarctica, *Bull. Volcanol.*, *56*(5), 361–376.
Paulsen, T. S., and T. J. Wilson (2010), Evolution of Neogene volcanism and stress patterns in the glaciated West Antarctic Rift, Marie Byrd Land, Antarctica, *J. Geol. Soc.*, *167*(2), 401–416.
Pollard, D., R. M. DeConto, and A. A. Nyblade (2005), Sensitivity of Cenozoic Antarctic ice sheet variations to geothermal heat flux, *Global Planet. Change*, *49*(1), 63–74.
Randall, D. E., and C. Mac Niocaill (2004), Cambrian palaeomagnetic data confirm a Natal Embayment location for the Ellsworth-Whitmore Mountains, Antarctica, in Gondwana reconstructions, *Geophys. J. Int.*, *157*(1), 105–116.
Rawlinson, N., and B. L. N. Kennett (2004), Rapid estimation of relative and absolute delay times across a network by adaptive stacking, *Geophys. J. Int.*, *157*(1), 332–340.
Ritzwoller, M. H., N. M. Shapiro, A. L. Levshin, and G. M. Leahy (2001), Crustal and upper mantle structure beneath, Antarctica and surrounding oceans, *J. Geophys. Res.*, *106*(B12), 30,645–30,670.
Roult, G., D. Rouland, and J. P. Montagner (1994), Antarctica II: Upper-mantle structure from velocities and anisotropy, *Phys. Earth Planet. Inter.*, *84*(1), 33–57.
Schmandt, B., K. Dueker, E. Humphreys, and S. Hansen (2012), Hot mantle upwelling across the 660 beneath Yellowstone, *Earth Planet. Sci. Lett.*, *331–332*, 224–236.
Schopf, J. M. (1969), Ellsworth mountains: Position in West Antarctica due to sea-floor spreading, *Science*, *164*(3875), 63–66.
Schroeder, D. M., D. D. Blankenship, D. A. Young, and E. Quartini (2014), Evidence for elevated and spatially variable geothermal flux beneath the West Antarctic Ice Sheet, *Proc. Natl. Acad. Sci. U.S.A.*, *111*(25), 9070–9072.
Shapiro, N. M., and M. H. Ritzwoller (2004), Inferring surface heat flux distributions guided by a global seismic model: Particular application to Antarctica, *Earth Planet. Sci. Lett.*, *223*(1), 213–224.
Shen, W., M. H. Ritzwoller, and V. Schulte-Pelkum (2013), A 3-D model of the crust and uppermost mantle beneath the Central and Western US by joint inversion of receiver functions and surface wave dispersion, *J. Geophys. Res. Solid Earth*, *118*, 262–276, doi:10.1029/2012JB009602.
Siddoway, C. S. (2008), Tectonics of the West Antarctic Rift System: New light on the history and dynamics of distributed intracontinental extension, in *Antarctica: A Keystone in a Changing World*, pp. 91–114, Natl. Acad. Press, Washington, D. C.
Sieminski, A., E. Debayle, and J. J. Lévêque (2003), Seismic evidence for deep low-velocity anomalies in the transition zone beneath West Antarctica, *Earth Planet. Sci. Lett.*, *216*(4), 645–661.
Sleep, N. H. (1990), Hotspots and mantle plumes: Some phenomenology, *J. Geophys. Res.*, *95*(B5), 6715–6736.
Steffen, H., G. Kaufmann, and P. Wu (2006), Three-dimensional finite-element modeling of the glacial isostatic adjustment in Fennoscandia, *Earth Planet. Sci. Lett.*, *250*(1), 358–375.
Storey, B. C., M. J. Hole, R. J. Pankhurst, I. L. Millar, and W. Vennum (1988), Middle Jurassic within-plate granites in West Antarctica and their bearing on the break-up of Gondwanaland, *J. Geol. Soc.*, *145*(6), 999–1007.
Sun, X., D. A. Wiens, A. Nyblade, S. Anandakrishnan, R. C. Aster, J. A. Chaput, A. D. Huerta, and T. J. Wilson (2013), Three-dimensional crust and upper mantle velocity structure of Antarctica from seismic noise correlation in *AGU Fall Meeting Abstracts* (vol. 1, p. 02).
Thurber, C. H. (1983), Earthquake locations and three-dimensional crustal structure in the Coyote Lake area, central California, *J. Geophys. Res.*, *88*(B10), 8226–8236.
Trey, H., A. K. Cooper, G. Pellis, B. della Vedova, G. Cochrane, G. Brancolini, and J. Makris (1999), Transect across the West Antarctic rift system in the Ross Sea, Antarctica, *Tectonophysics*, *301*(1), 61–74.
Um, J., and C. Thurber (1987), A fast algorithm for two-point seismic ray tracing, *Bull. Seismol. Soc. Am.*, *77*(3), 972–986.
van der Wal, W., P. L. Whitehouse, and E. J. Schrama (2015), Effect of GIA models with 3D composite mantle viscosity on GRACE mass balance estimates for Antarctica, *Earth Planet. Sci. Lett.*, *414*, 134–143.
Van Wijk, J., W. Baldridge, J. van Hunen, S. Goes, R. Aster, D. Coblentz, S. Grand, and J. Ni (2010), Small-scale convection at the edge of the Colorado Plateau: Implications for topography, magmatism, and evolution of Proterozoic lithosphere, *Geology*, *38*, 611–614.
Veevers, J. J. (2012), Reconstructions before rifting and drifting reveal the geological connections between Antarctica and its conjugates in Gondwanaland, *Earth Sci. Rev.*, *111*(3), 249–318.
Walcott, R. I. (1970), Isostatic response to loading of the crust in Canada, *Can. J. Earth Sci.*, *7*(2), 716–727.
Wannamaker, P. E., J. A. Stodt, and S. L. Olsen (1996), Dormant state of rifting below the Byrd Subglacial Basin, West Antarctica, implied by magnetotelluric (MT) profiling, *Geophys. Res. Lett.*, *23*(21), 2983–2986.
Watson, T., A. Nyblade, D. A. Wiens, S. Anandakrishnan, M. Benoit, P. J. Shore, D. Voigt, and J. VanDecar (2006), *P* and *S* velocity structure of the upper mantle beneath the Transantarctic Mountains, East Antarctic craton, and Ross Sea from travel time tomography, *Geochem. Geophys. Geosyst.*, *7*, Q07005, doi:10.1029/2005GC001238.
Wessel, P., and W. H. Smith (1998), New, improved version of Generic Mapping Tools released, *Eos Trans. AGU*, *79*(47), 579–579.
Wiens, D. A., J. A. Conder, and U. H. Faul (2008), The seismic structure and dynamics of the mantle wedge, *Ann. Rev. Earth Planet. Sci.*, *36*, 421–455.
Wilson, D. S., and B. P. Luyendyk (2009), West Antarctic paleotopography estimated at the Eocene-Oligocene climate transition, *Geophys. Res. Lett.*, *36*, L16302, doi:10.1029/2009GL039297.
Wilson, D., R. Aster, M. West, J. Ni, S. Grand, W. Gao, W. S. Baldridge, S. Semken, and P. Patal (2005), Lithospheric structure of the Rio Grande rift, *Nature*, *433*, 851–855.
Wilson, T., et al. (2015), Understanding glacial isostatic adjustment and ice mass change in Antarctica using integrated GPS and seismology observations European Geophysical Union Annual Meeting Supplement.
Winberry, J. P., and S. Anandakrishnan (2003), Seismicity and neotectonics of West Antarctica, *Geophys. Res. Lett.*, *30*(18), 1931, doi:10.1029/2003GL018001.

Winberry, J. P., and S. Anandakrishnan (2004), Crustal structure of the West Antarctic rift system and Marie Byrd Land hotspot, *Geology*, *32*(11), 977–980.

Zhao, D. (1991), A tomographic study of seismic velocity structure in the Japan Islands, Doctoral dissertation, Tōhoku Univ.

Zhao, D., A. Hasegawa, and S. Horiuchi (1992), Tomographic imaging of *P* and *S* wave velocity structure beneath northeastern Japan, *J. Geophys. Res.*, *97*(B13), 19,909–19,928.

Zhao, D., A. Hasegawa, and H. Kanamori (1994), Deep structure of Japan subduction zone as derived from local, regional, and teleseismic events, *J. Geophys. Res.*, *99*(B11), 22,313–22,329.